Supporting Information

Diastereoselectively self-sorted low-symmetry binuclear metallomacrocycle and trinuclear metallocage

Srabani Srotoswini Mishra[a] and Dillip Kumar Chand*[a]

[a] Department of Chemistry, Indian Institute of Technology Madras, Chennai 600036, India,

E-mail: dillip@iitm.ac.in

Table of contents

Captions of Supporting Figures, Tables and Schemes

Fig. S10a. 500 MHz H-H COSY expansion spectrum of complex, **1** in DMSO-d_6.

Fig. S11. 500 MHz C-H COSY spectrum of complex, **1** in DMSO-d_6.

Fig. S11a. 500 MHz C-H COSY expansion spectrum of complex, **1** in DMSO-d_6.

Fig. S11b. 500 MHz C-H COSY expansion spectrum (showing -CH_2 peak position corresponding to *cis*-protecting group, ethylenediamine) of complex, **1** in DMSO-d_6.

Fig. S12. 500 MHz NOESY expansion spectrum of cage, **1** in DMSO-d_6.

Fig. S12a. 500 MHz NOESY expansion spectrum of cage, **1** in DMSO-d_6.

Table S1. Summary of crystallographic data for complex **1**.

Fig. S13. ORTEP of the molecule in crystals of **1**. Thermal ellipsoids are drawn at 40% probability. Hydrogen atoms and counter anions have been omitted for clarity.

Fig. S14. Optimized geometries and relative energies of the possible isomers of $[Pd_2(en)_2(\mathbf{L^{un}})_2]^{4+}$ in implicit DMSO phase.

Table S2. Energy values of the possible isomers of the complexed cation, $[Pd_2(en)_2(\mathbf{L^{un}})_2]^{4+}$ in gas phase: [B3LYP-D3/SDD,6-31G(d)].

Table S3. Energy values of the possible isomers of the complexed cation, $[Pd_2(en)_2(\mathbf{L^{un}})_2]^{4+}$ in implicit DMSO phase: [B3LYP-D3/SDD,6-31G(d)].

Scheme S1. Synthesis of the low symmetry trinuclear complex all-*cis*(2,2)- or all-*trans*(2,2)-$[Pd_3(\mathbf{L^{un}})_6](NO_3)_6$, **2** with minor amount of proposed low symmetry tetranuclear complex $[Pd_4(\mathbf{L^{un}})_8](NO_3)_8$, **3** (concentration: 10 Mm with respect to palladium(II)).

Fig. S15. Optimized geometries and relative energies of all-*cis*(2,2)-$[Pd_3(\mathbf{L^{un}})_6]^{6+}$ and all-*trans*(2,2)-$[Pd_3(\mathbf{L^{un}})_6]^{6+}$ (where ligand conformation is either all *syn-syn* or all-*anti-anti*) in gas phase.

Table S4: Energy values of the possible isomers of the complexed cation, $[Pd_3(L^{un})_6]^{6+}$: [B3LYP-D3/SDD,6-31G(d)].

Fig. S16. 400 MHz ^{1}H NMR spectrum of complex, **2+3** in DMSO-d_6.

Fig. S17. 125 MHz ^{13}C NMR spectrum of complex, **2+3** in DMSO-d_6.

Fig. S17a. 125 MHz ^{13}C NMR expansion spectrum of complex, **2+3** in DMSO-d_6.

Fig. S18. 500 MHz H-H COSY spectrum of complex, **2+3** in DMSO-d_6.

Fig. S18a. 500 MHz H-H COSY expansion spectrum of complex, **2**+**3** in DMSO-d_6.

Fig. S19. 500 MHz C-H COSY spectrum of complex, **2**+**3** in DMSO-d_6.

Fig. S19a. 500 MHz C-H COSY expansion spectrum of complex, **2**+**3** in DMSO-d_6.

Fig. S20. 500 MHz NOESY spectrum of complex, **2**+**3** in DMSO-d_6.

Fig. S20a. 500 MHz NOESY expansion spectrum of complex, **2**+**3** in DMSO-d_6.

Fig. S21. Partial 400 MHz ^{1}H NMR spectra of the sample obtained from complexation of $Pd(NO_3)_2$ and ligand $\mathbf{L^{un}}$ mixed in 1:2 ratio at 2.5 mM recorded at (i) rt (ii) 70 ºC (iii) rt (reached by cooling down) in DMSO-d_6. (Concentration: 2.5 mM with respect to palladium(II)).

Fig. S22. Partial 400 MHz ^{1}H NMR spectra of (i) ligand, $\mathbf{L^{un}}$; (ii) to (v) sample obtained from the complexation of $Pd(NO_3)_2$ and ligand $\mathbf{L^{un}}$ mixed in 1:2 ratio at (ii) 2.5 mM; (iii) 5 mM; (iv) 10 mM; (v) 60 mM in DMSO-d_6. (Concentration: 2.5 to 60 mM range, with respect to palladium(II)).

Table S5. Approximate percentage of $\mathbf{L^{un}}$ in the complexes **2** and **3** at various concentration as calculated from integration ratio of suitable ^{1}H NMR signals.

Fig. S23. Partial 500 MHz variable temperature ^{1}H NMR spectra of **2**+**3** recorded at (i) rt ; (ii) 40 ºC; (iii) 50 ºC; (iv) 60 ºC; (v) 70 ºC; (vi) 80 ºC; (vii) 90 ºC; and (viii) rt (reached by cooling down) in DMSO-d_6. (Concentration: 10 mM with respect to palladium(II)).

Fig. S24. Partial 400 MHz ^{1}H NMR spectra of **2**+**3** monitored after aging for (i) 1 d; (ii) 2 d; and (iii) 10 d in DMSO-d_6. (Concentration: 10 mM with respect to palladium(II)).

Fig. S25. Partial 400 MHz ^{1}H NMR spectra of (i) ligand $\mathbf{L^{un}}$; (ii) all-*cis*(2,2)- or all-*trans*(2,2)-$[Pd_3(\mathbf{L^{un}})_6](NO_3)_6$, **2** (iii) **all-***cis*(2,2)- or all-*trans*(2,2)-$[Pd_3(\mathbf{L^{un}})_6](BF_4)_6$, **2'** in DMSO-$d_6$. (Concentration: 2.5 mM with respect to palladium(II))

Fig. S26. ESI-MS spectrum of trinuclear complex $[Pd_3(\mathbf{L^{un}})_6](BF_4)_6$, **2'** and tetranuclear complex $[Pd_4(\mathbf{L^{un}})_8](BF_4)_8$, **3'**.

Fig. S26a. Experimental (top) and simulated (bottom) ESI-MS isotopic peak patterns corresponding to the cation $[\mathbf{2'}\text{-}2BF_4]^{2+}$.

Fig. S26b. Experimental (top) and simulated (bottom) ESI-MS isotopic peak patterns corresponding to the cation $[\mathbf{2'}\text{-}3BF_4]^{3+}$.

Fig. S26c. Experimental (top) and simulated (bottom) ESI-MS isotopic peak patterns corresponding to the cation [**3'**-3BF_4]$^{3+}$.

Fig. S27. Partial 400 MHz ^{1}H spectra of (i) all (1,1)-[$Pd_2(en)_2$(**L^{un}**)$_2$]$(NO_3)_4$, **1**; (ii)-(iv) monitoring the formation of a mixture of all-*cis*(2,2)- or all-*trans*(2,2)-[Pd_3(**L^{un}**)$_6$]$(NO_3)_6$, **2** and $Pd(en)_2(NO_3)_2$, **4** by standing a solution of **1** at ambient temperature for (ii) 3 d; (iii) 9 d; (iv) 14 d; (v) freshly prepared **2**, in DMSO-d_6. A dynamic equilibrium of **1** (65% with respect to ligand) with a mixture of **2** (35% with respect to ligand) and **4** was observed.

Fig. S28. Partial 400 MHz ^{1}H spectra of (i) *cis*(2,2)- or *trans*(2,2)-[Pd_3(**L^{un}**)$_6$]$(NO_3)_6$, **2**; (ii)-(v) monitoring the formation of (1,1)-[$Pd_2(en)_2$(**L^{un}**)$_2$]$(NO_3)_4$, **1** from a mixture of **2** and $Pd(en)_2(NO_3)_2$, **4** by standing at ambient temperature for (ii) 3 d; (iii) 6 d; (iv) 14 d; (v) freshly prepared **1**, in DMSO-d_6. A dynamic equilibrium of **1** (75% with respect to ligand) with a mixture of **2** (25% with respect to ligand) and **4** was observed.

SUPPORTING DATA

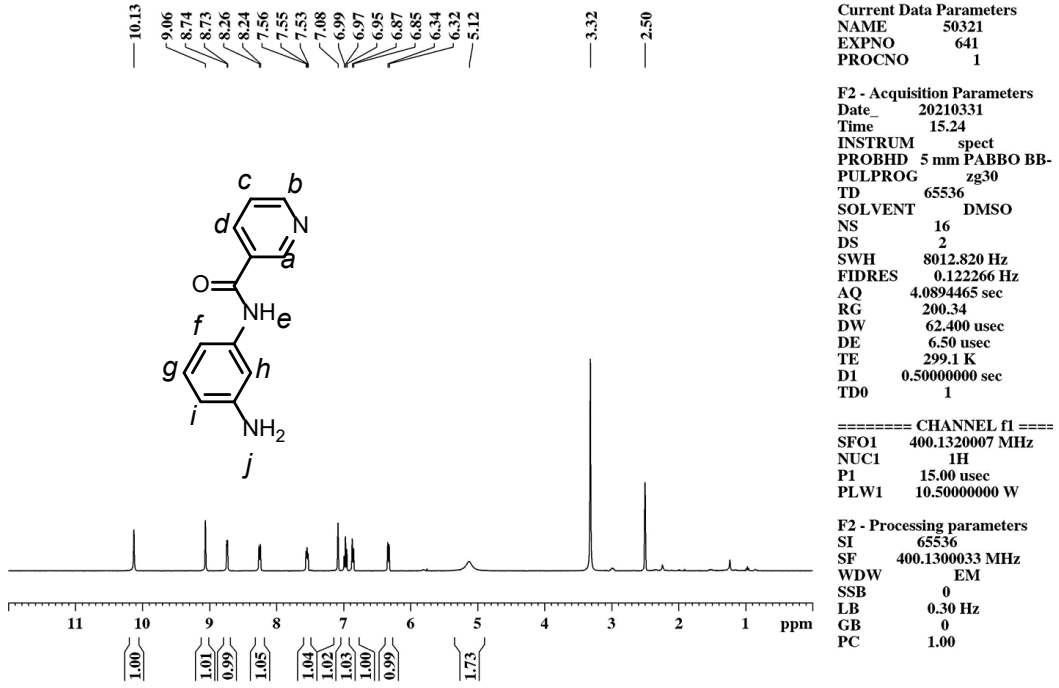

Fig. S1. 400 MHz ^{1}H NMR spectrum of ligand, $\mathbf{L^{un}}$ in DMSO-d_6.

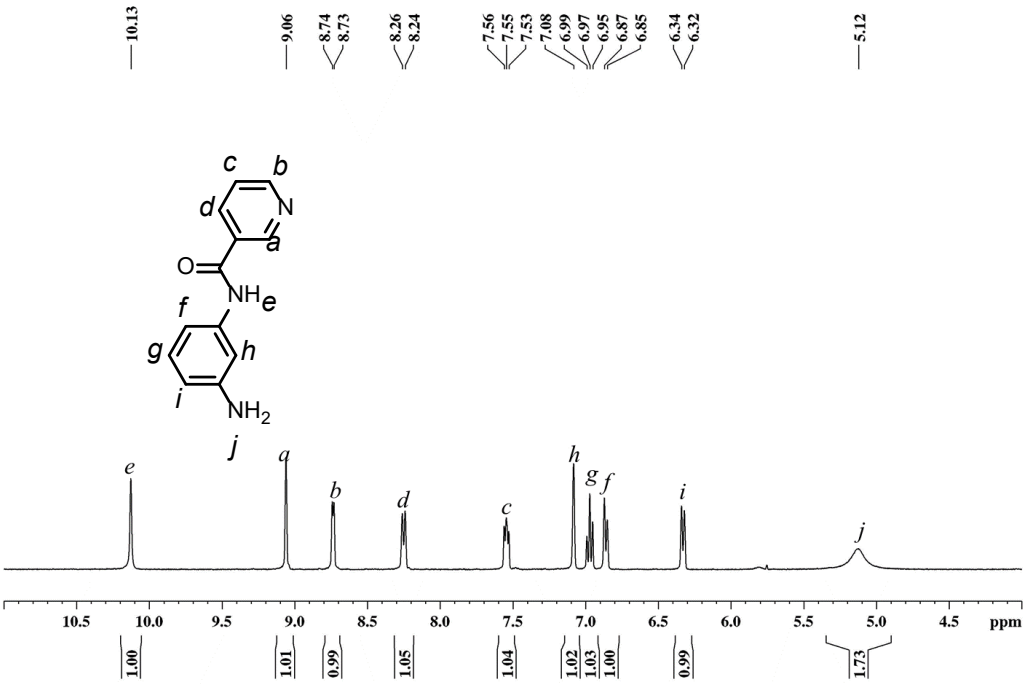

Fig. S1a. 400 MHz ^{1}H NMR expansion spectrum of ligand, $\mathbf{L^{un}}$ in DMSO-d_6.

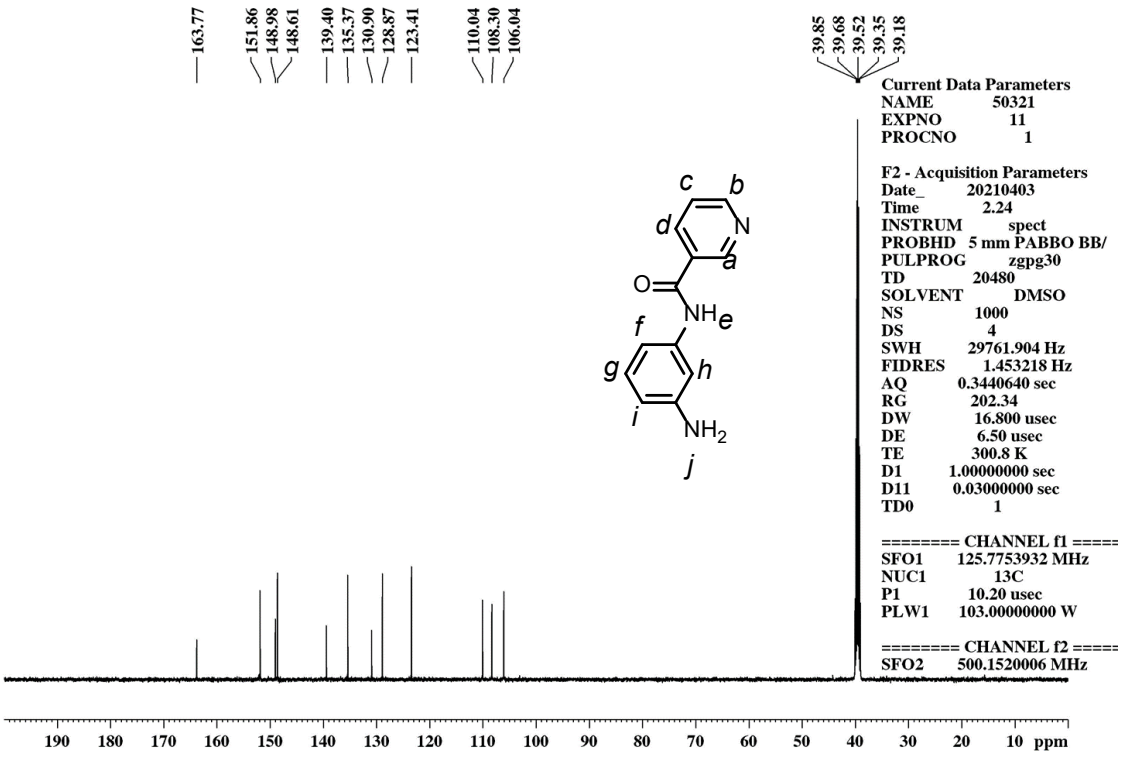

Fig. S2. 125 MHz ^{13}C NMR spectrum of ligand, $\mathbf{L^{un}}$ in DMSO-d_6.

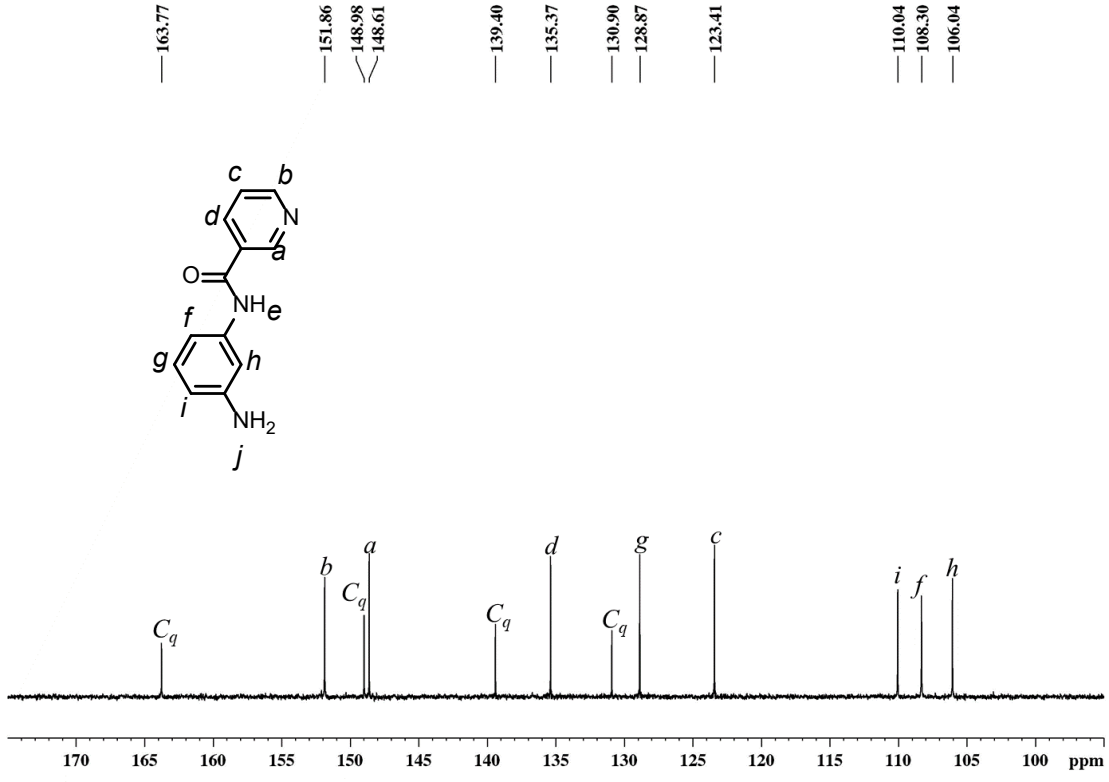

Fig. S2a. 125 MHz ^{13}C NMR expansion spectrum of ligand, $\mathbf{L^{un}}$ in DMSO-d_6.

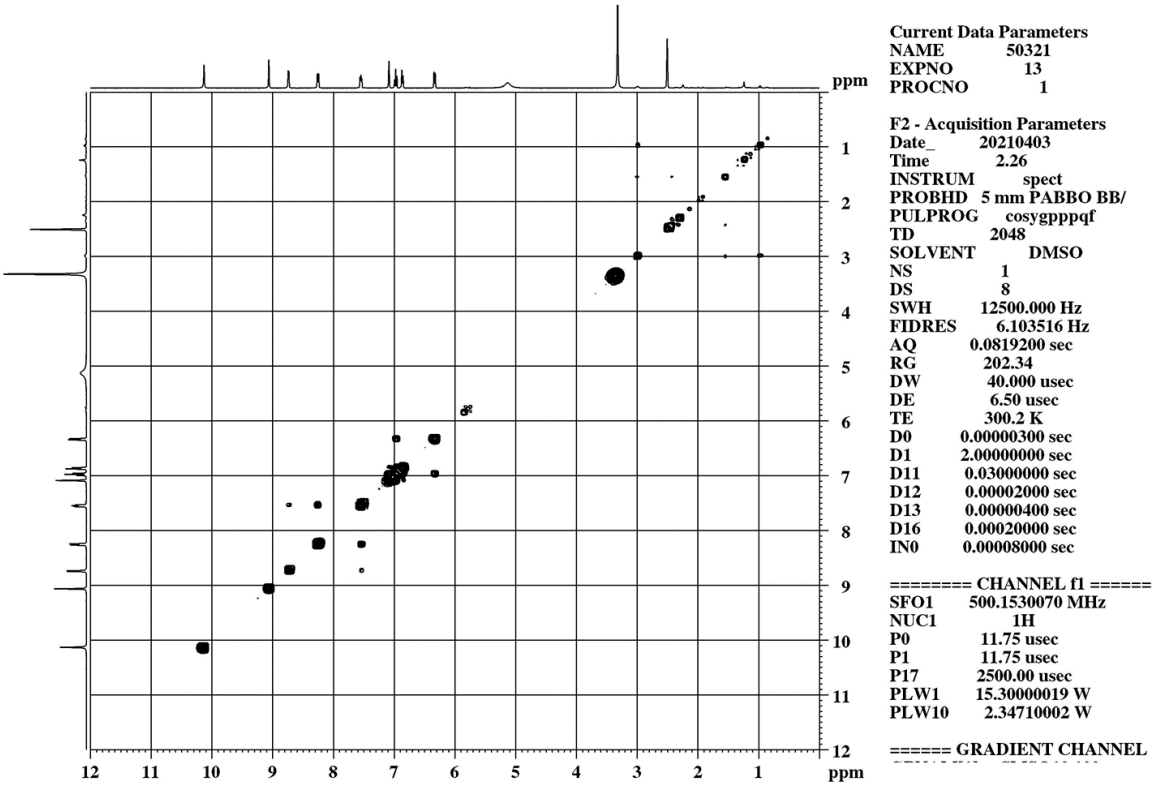

Fig. S3. 500 MHz H-H COSY spectrum of ligand, $\mathbf{L^{un}}$ in DMSO-d_6.

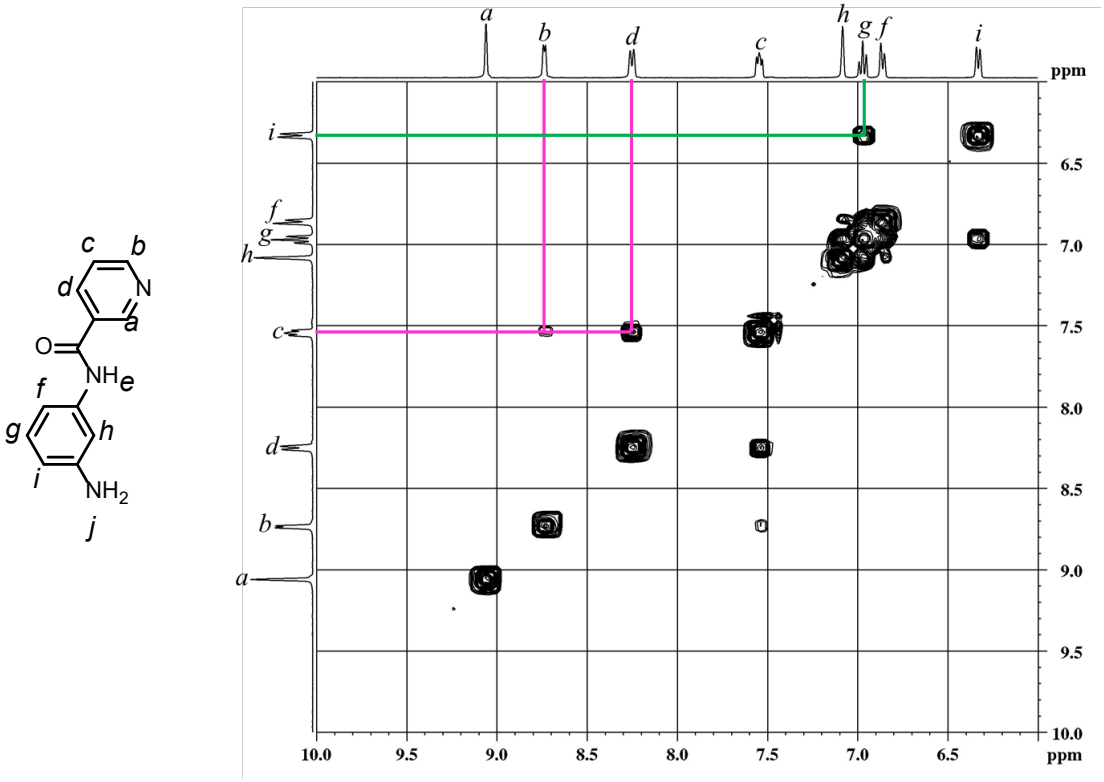

Fig. S3a 500 MHz H-H COSY expansion spectrum of ligand, $\mathbf{L^{un}}$ in DMSO-d_6.

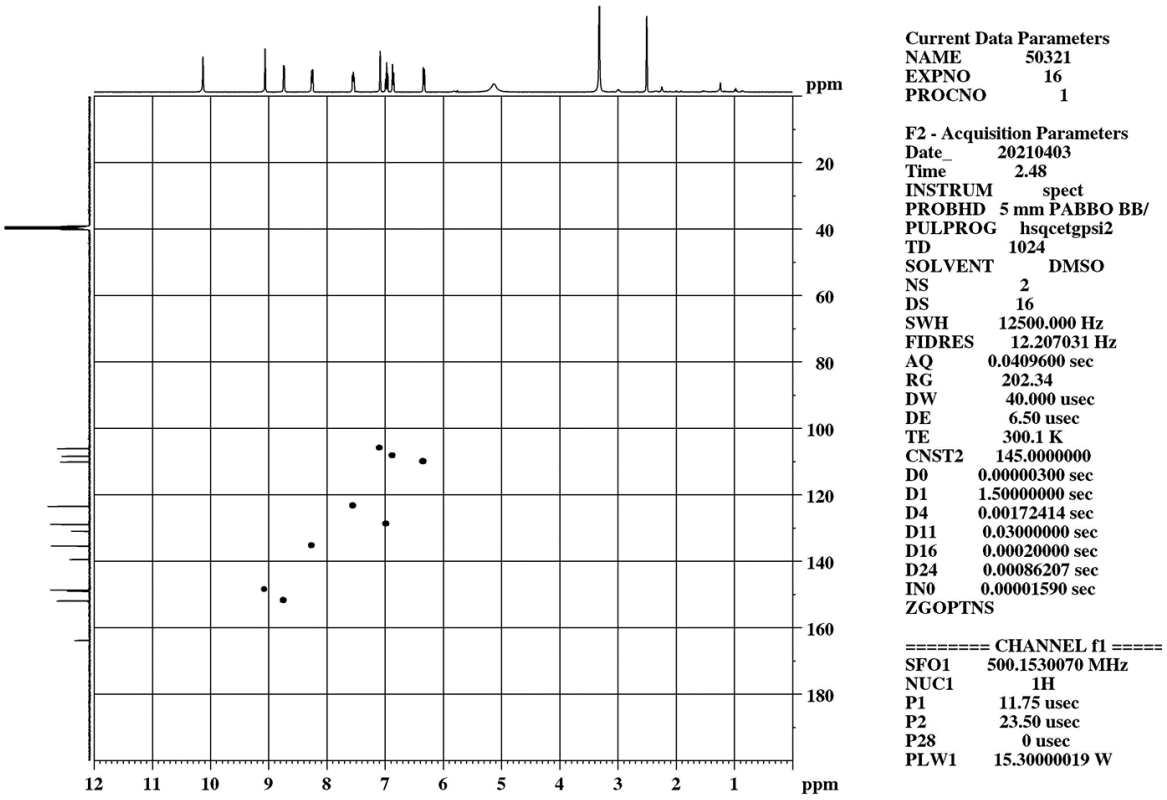

Fig. S4. 500 MHz C-H COSY spectrum of ligand, $\mathbf{L^{un}}$ in DMSO-d_6.

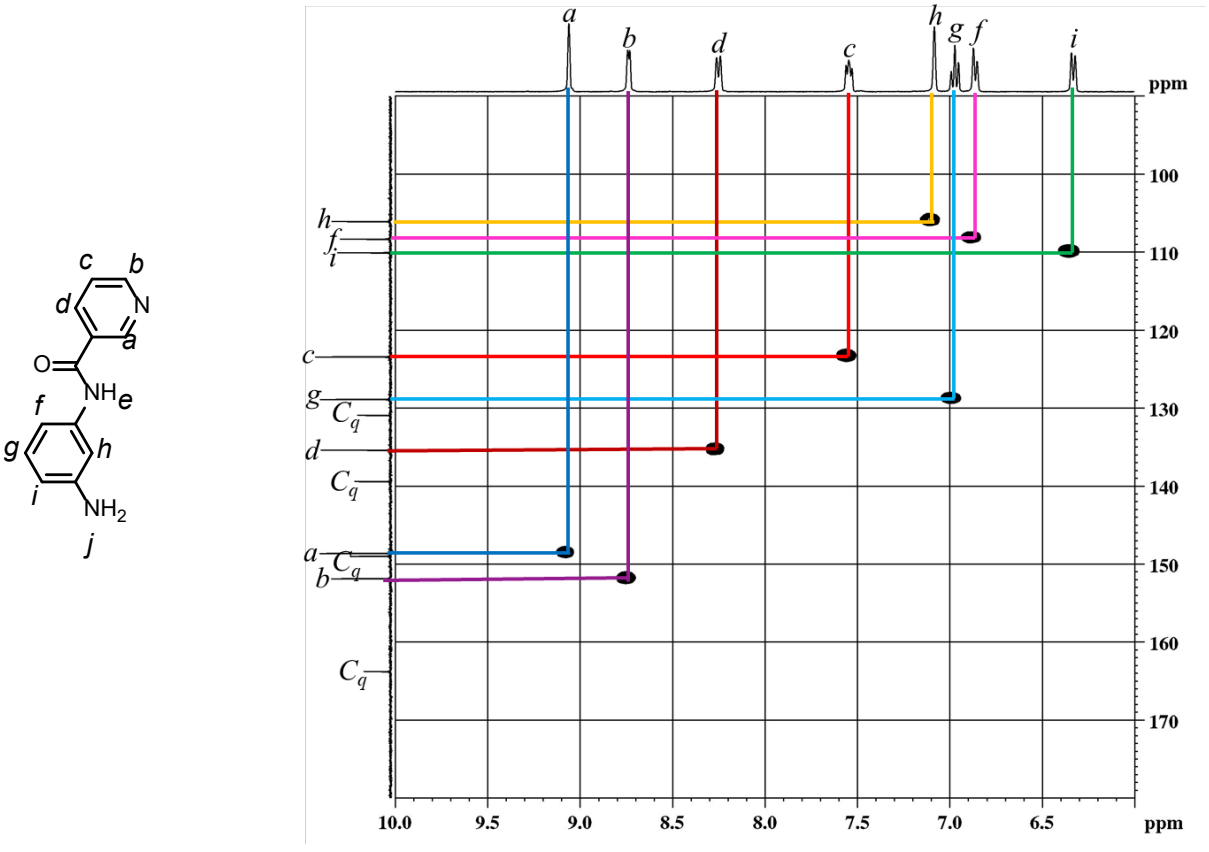

Fig. S4a. 500 MHz C-H COSY expansion spectrum of ligand, $\mathbf{L^{un}}$ in DMSO-d_6.

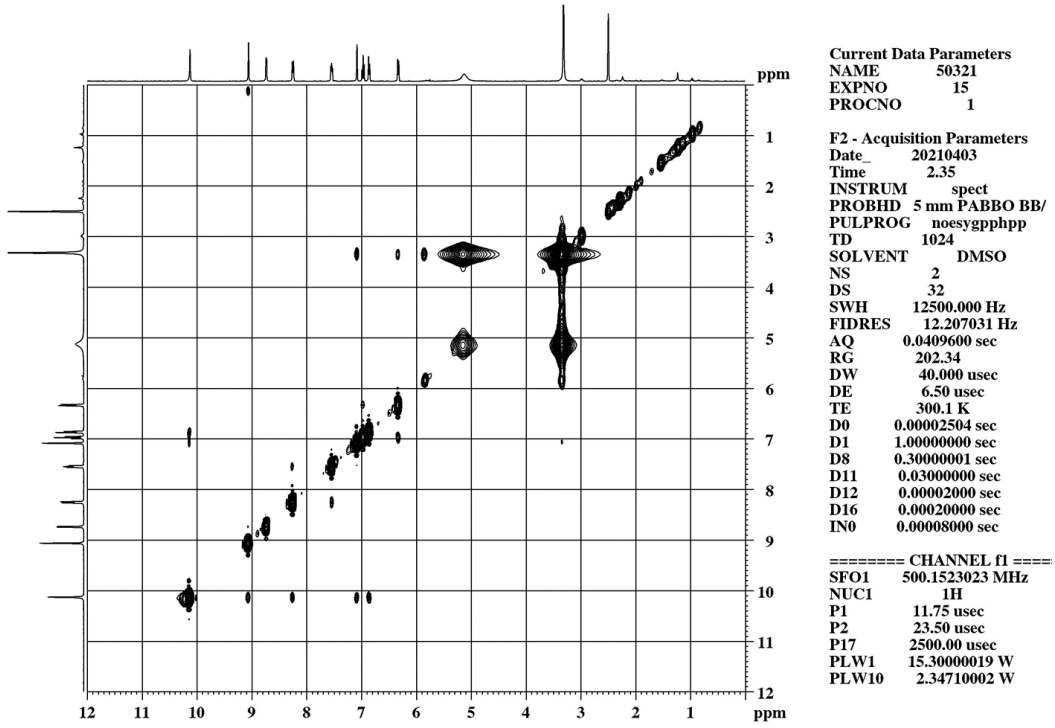

Fig. S5. 500 MHz H-H NOESY spectrum of ligand, $\mathbf{L^{un}}$ in DMSO-d_6.

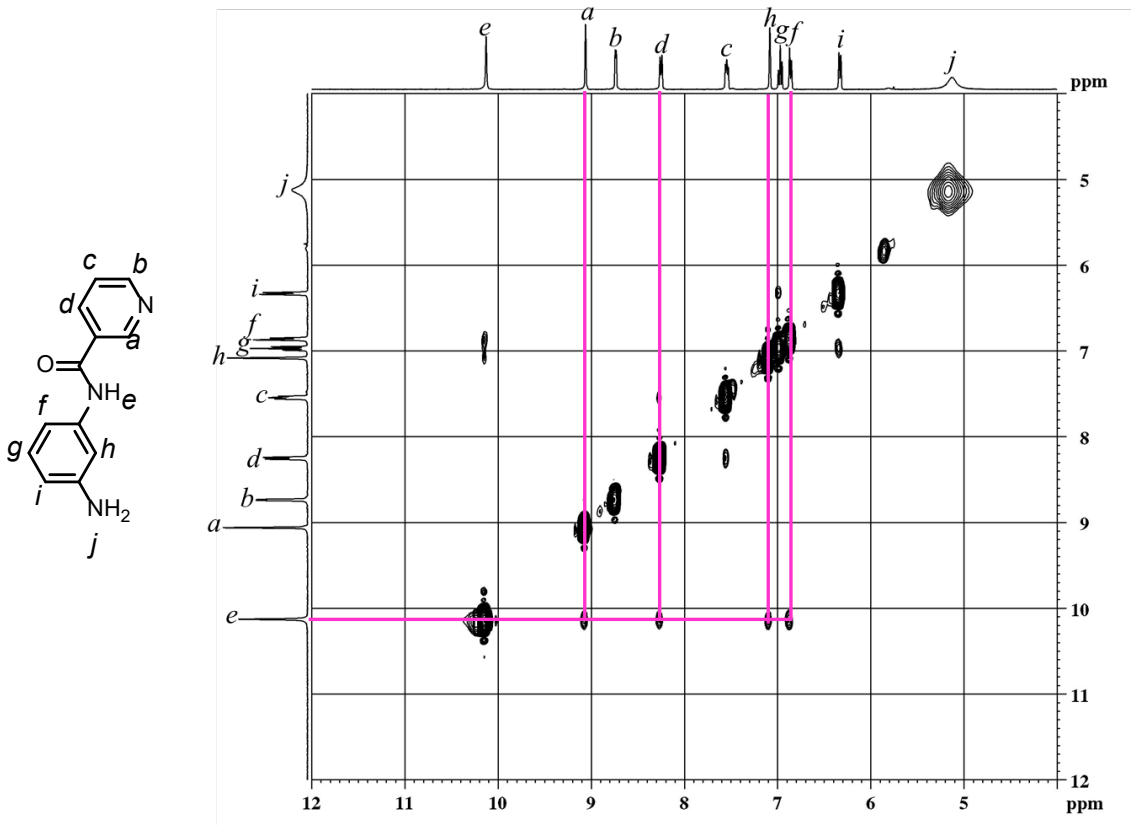

Fig. S5a. 500 MHz H-H NOESY expansion spectrum of ligand, $\mathbf{L^{un}}$ in DMSO-d_6.

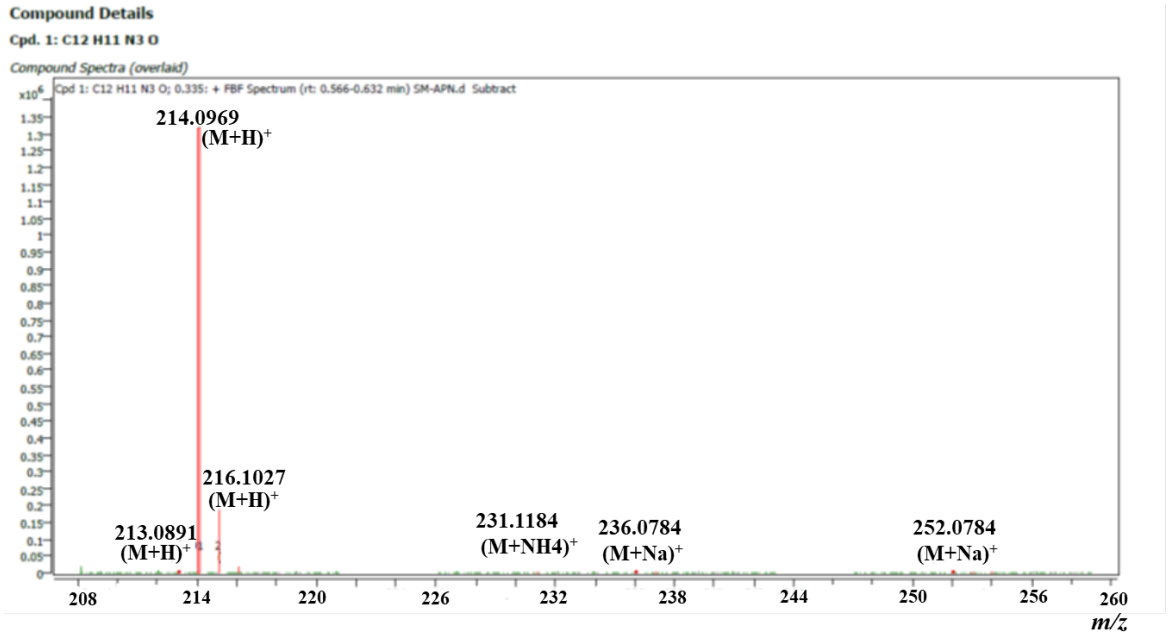

Fig. S6. ESI-MS data of ligand, $\mathbf{L^{un}}$.

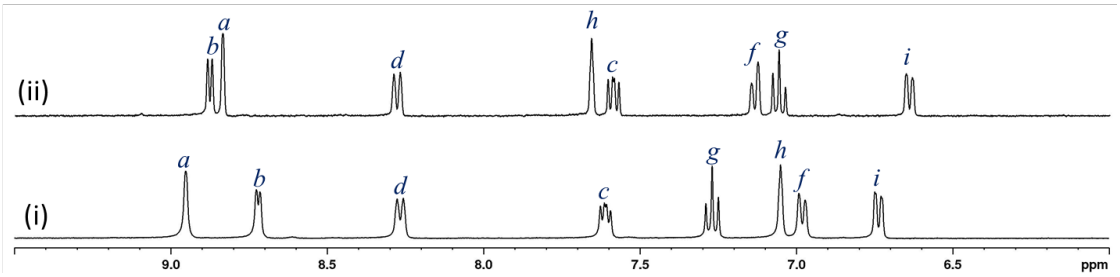

Fig. S7. Partial 400 MHz ^{1}H NMR spectra of (i) ligand, $\mathbf{L^{un}}$; (ii) sample obtained from equimolar combination of $Pd(en)(NO_3)_2$ and ligand $\mathbf{L^{un}}$ in D_2O. (Concentration: 10 mM with respect to palladium(II)).

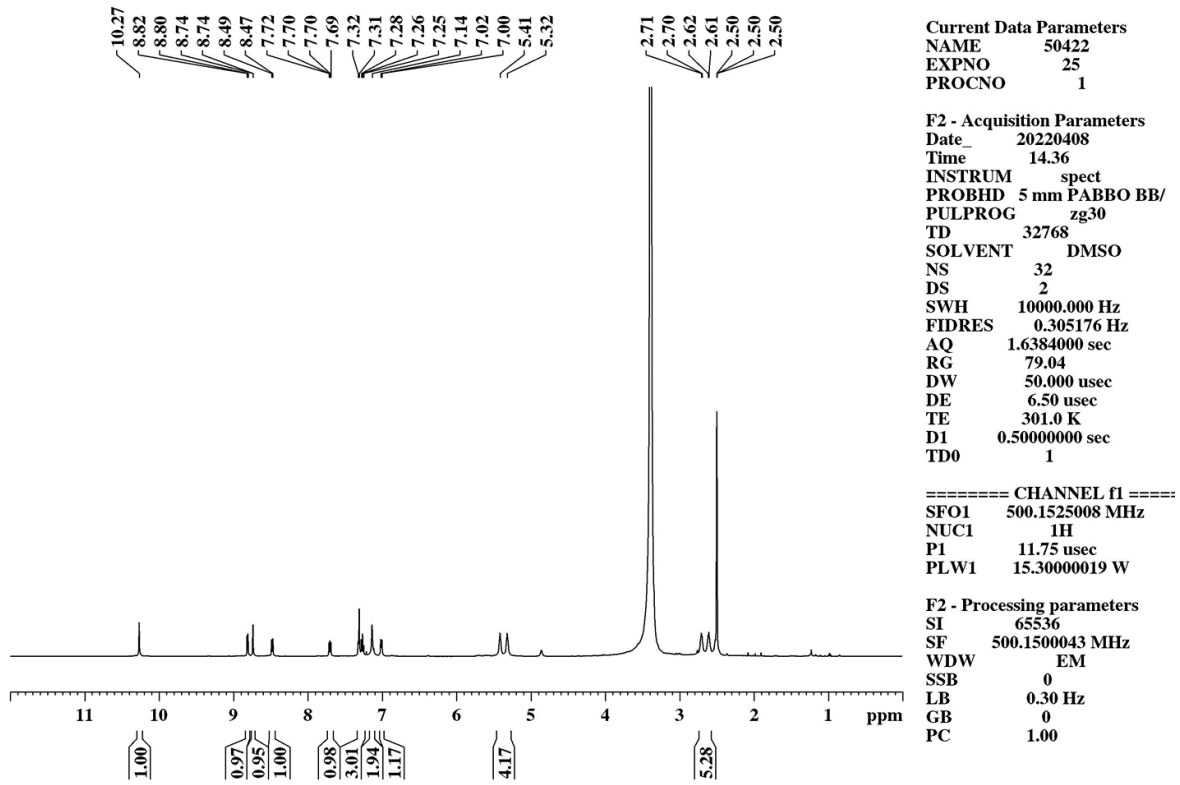

Fig. S8. 400 MHz ^{1}H NMR spectrum of complex, **1** in DMSO-d_6.

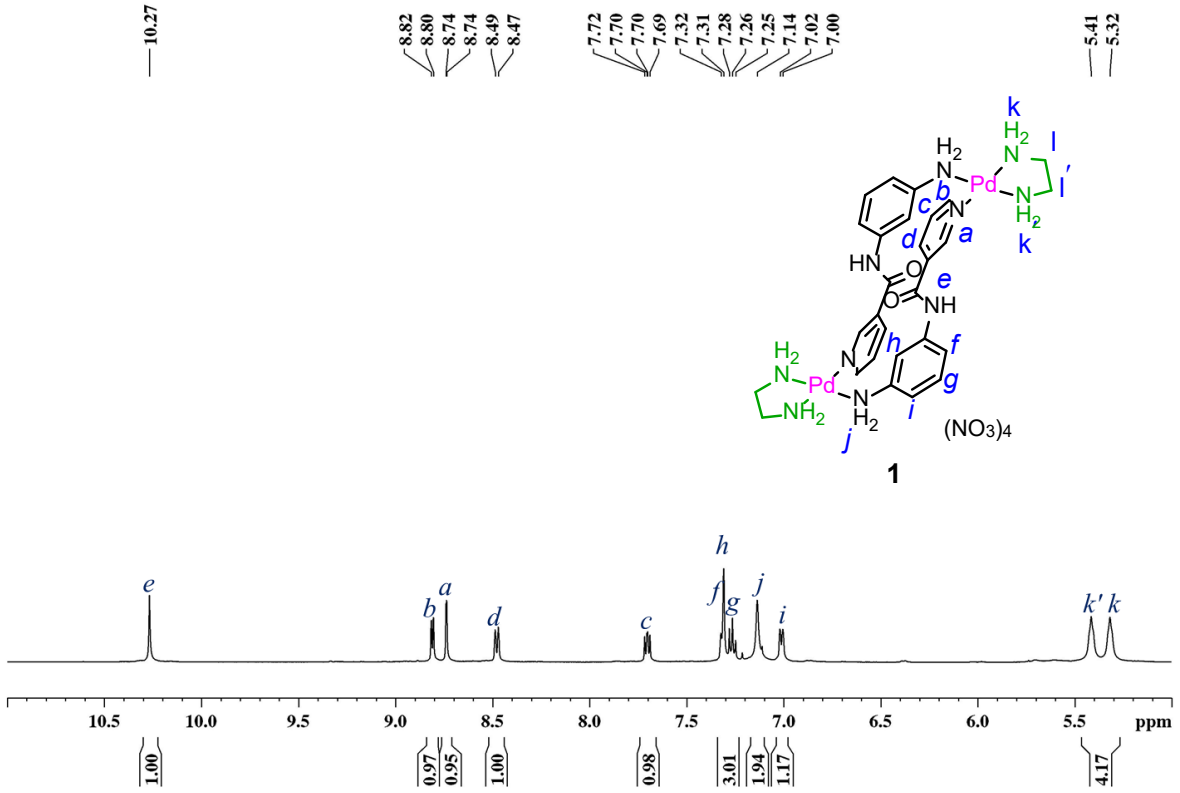

Fig. S8a. 400 MHz ^{1}H NMR expansion spectrum of complex, **1** in DMSO-d_6.

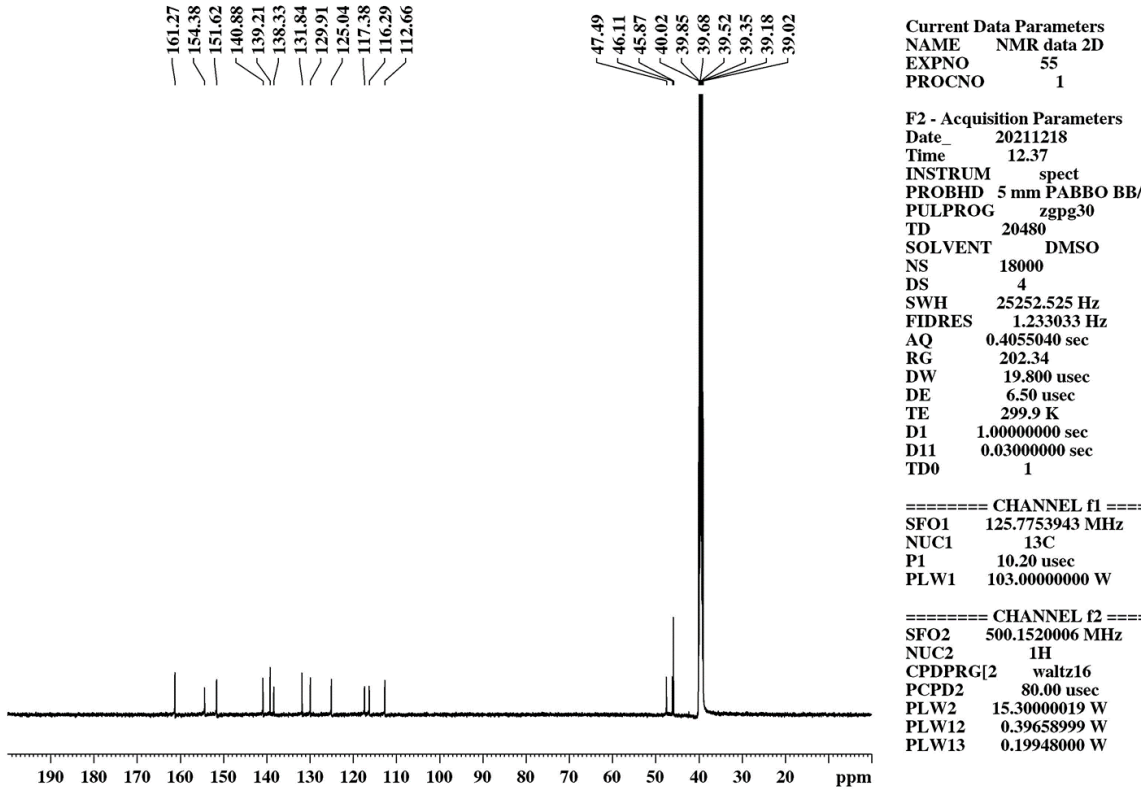

Fig. S9. 125 MHz ^{13}C NMR spectrum complex, **1** in DMSO-d_6.

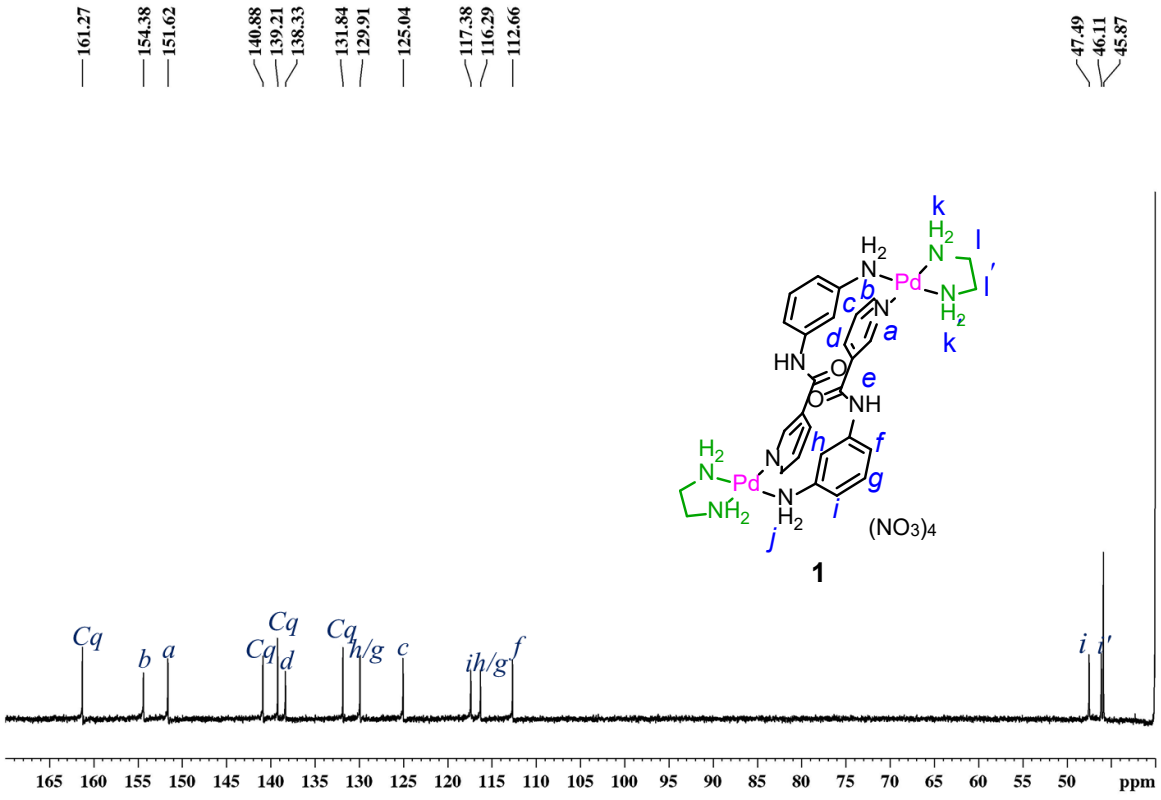

Fig. S9a. 125 MHz ^{13}C NMR expansion spectrum complex, **1** in DMSO-d_6.

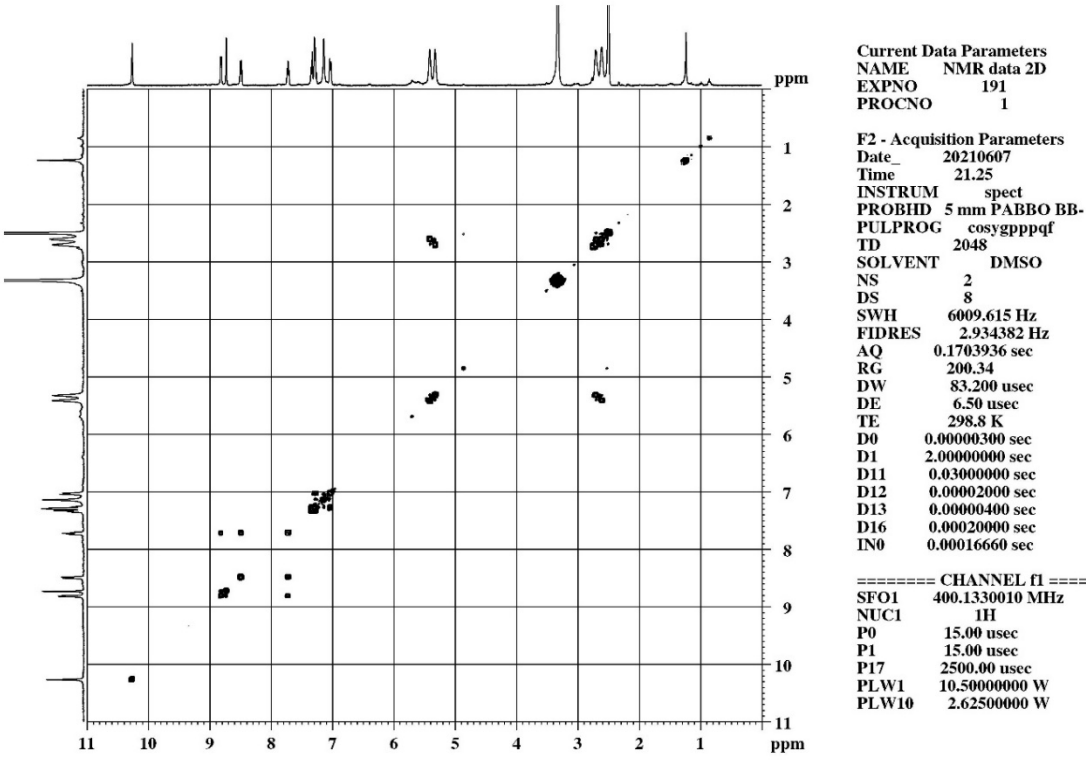

Fig. S10. 500 MHz H-H COSY spectrum of complex, **1** in DMSO-d_6.

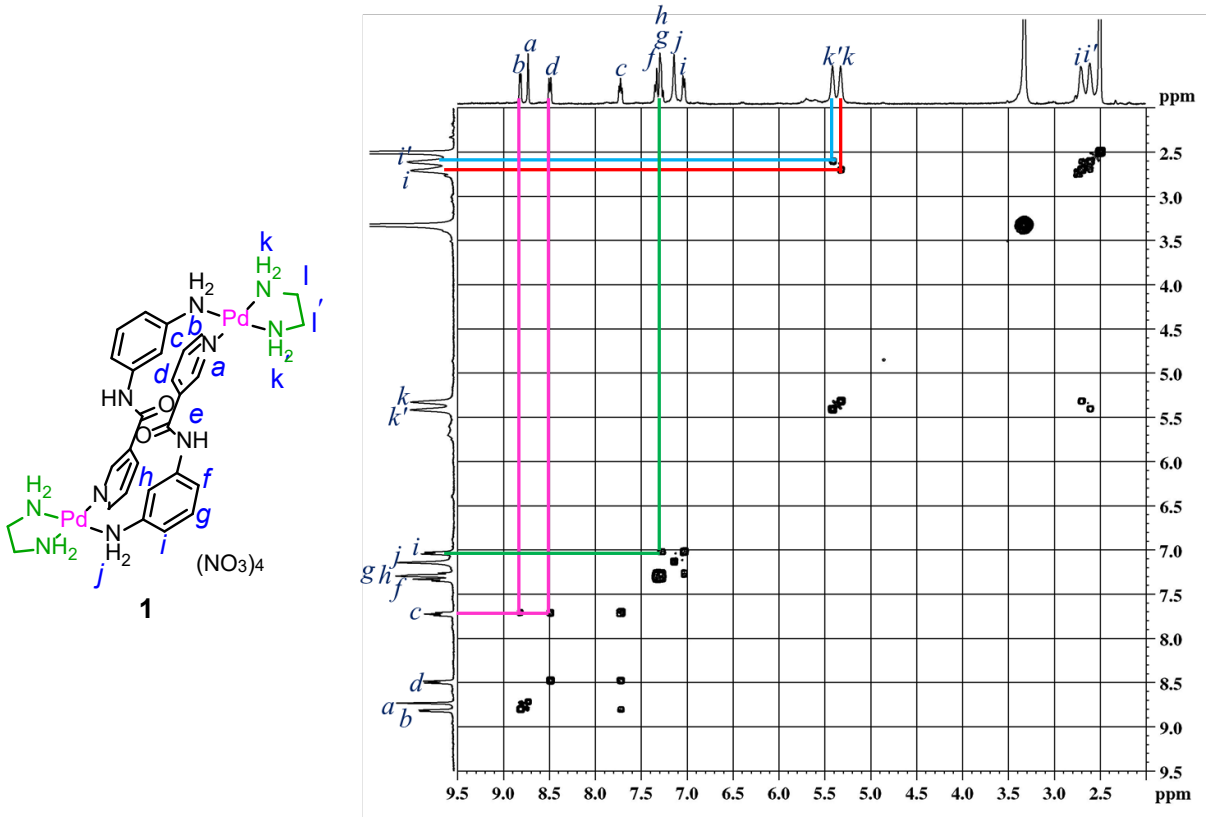

Fig. S10a. 500 MHz H-H COSY expansion spectrum of complex, **1** in DMSO-d_6.

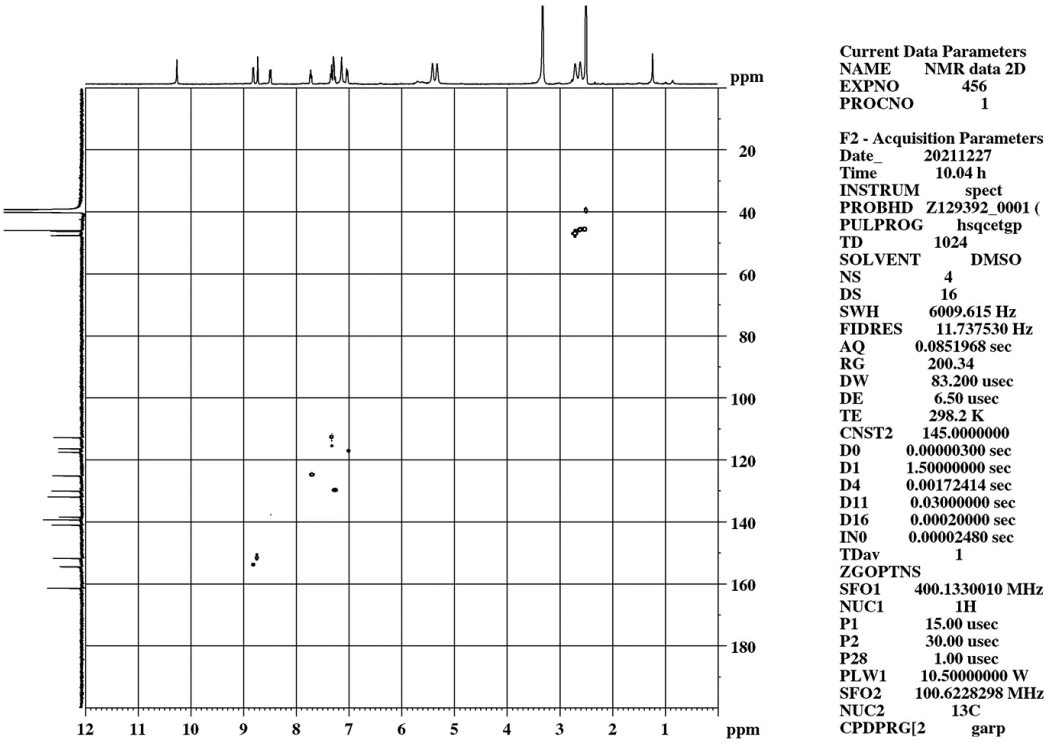

Fig. S11. 500 MHz C-H COSY spectrum of complex, **1** in DMSO-d_6.

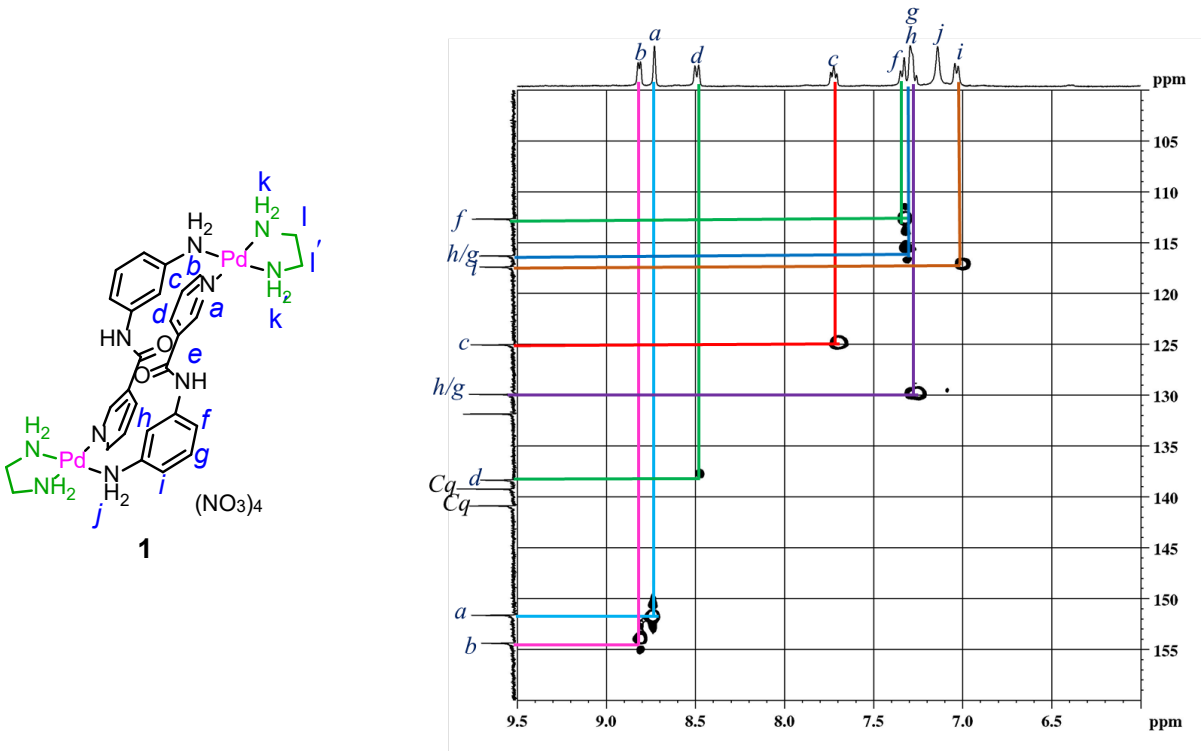

Fig. S11a. 500 MHz C-H COSY expansion spectrum of complex, **1** in DMSO-d_6.

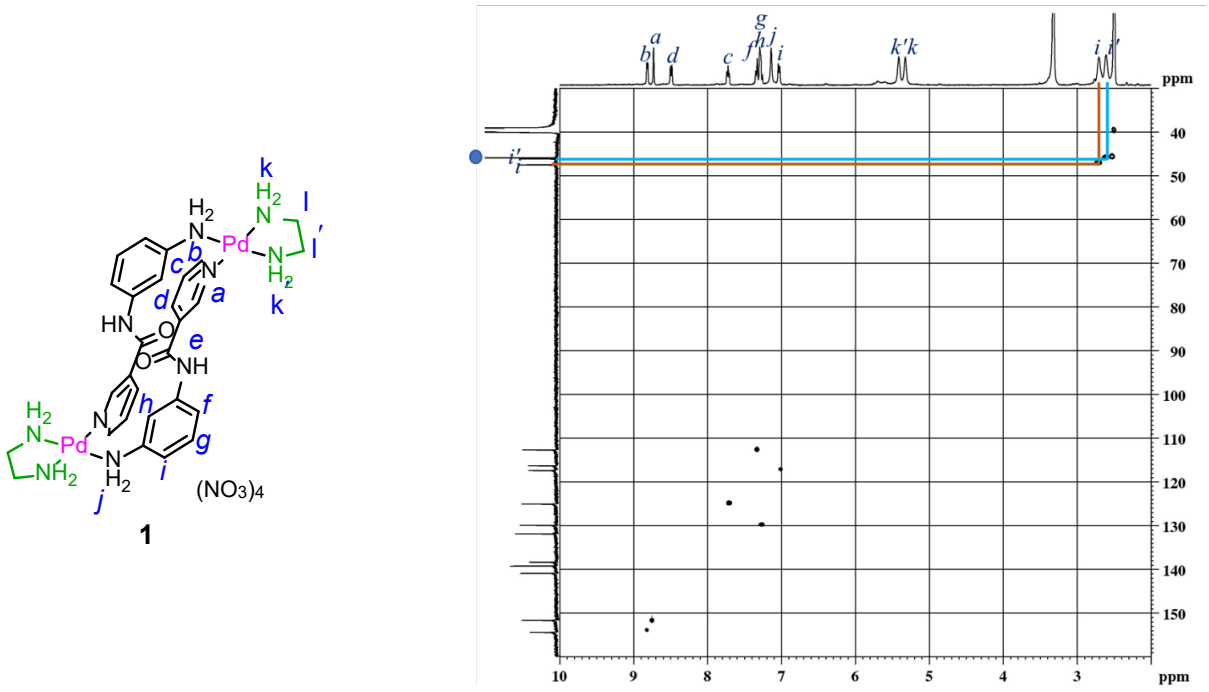

Fig. S11b. 500 MHz C-H COSY expansion spectrum (showing -CH_2 peak position corresponding to *cis*-protecting group, ethylenediamine) of complex, **1** in DMSO-d_6.

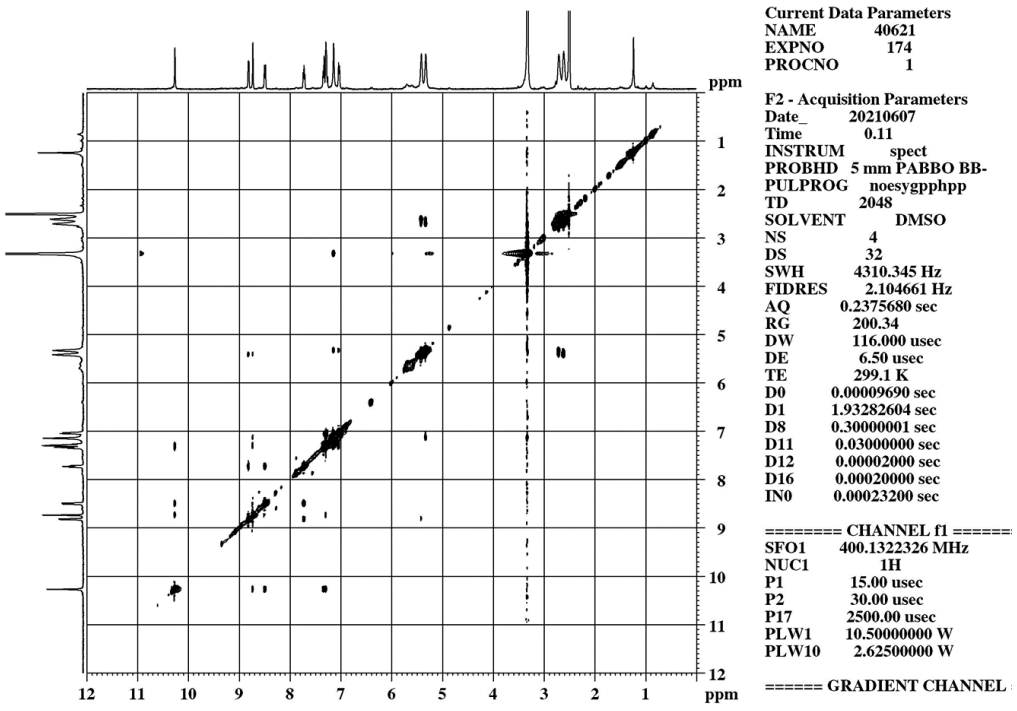

Fig. S12. 500 MHz NOESY expansion spectrum of cage, **1** in DMSO-d_6.

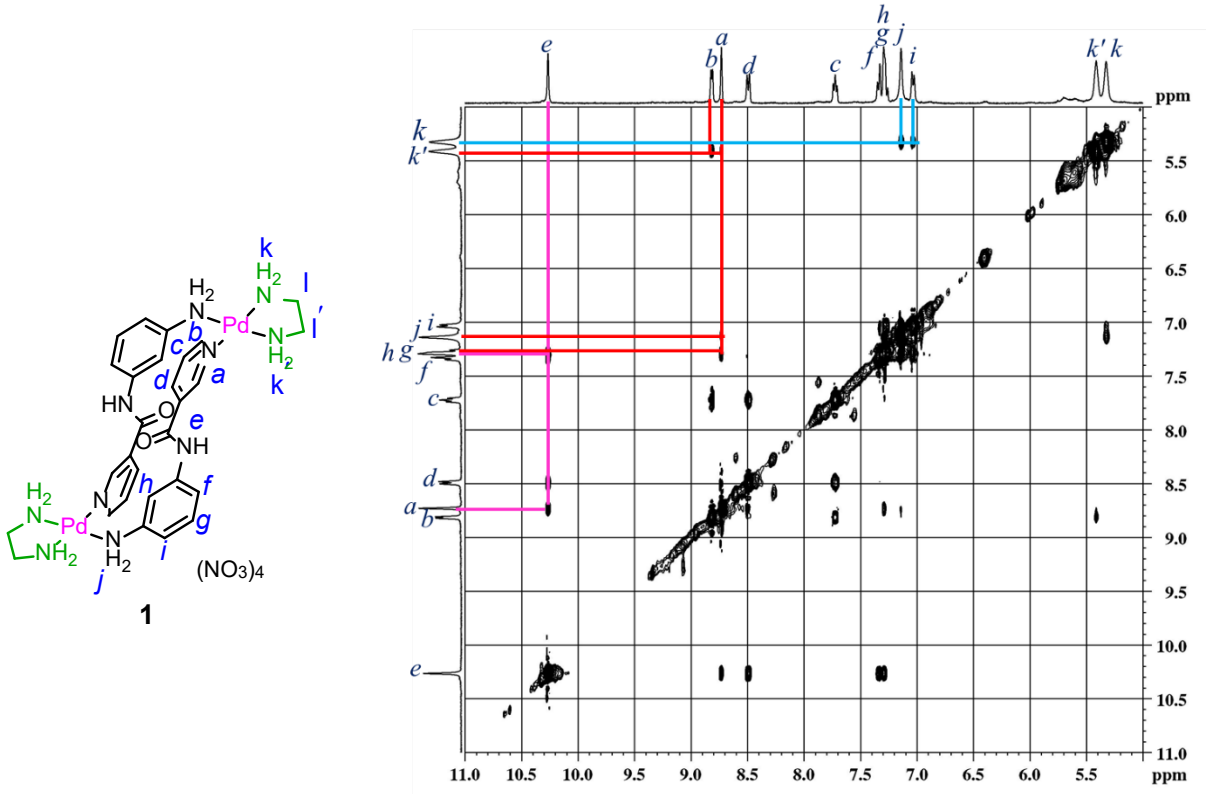

Fig. S12a. 500 MHz NOESY expansion spectrum of cage, **1** in DMSO-d_6.

Crystallographic Data: X-ray diffraction-quality single crystals of **1** was obtained by the slow evaporation of an aqueous solution of cage **1**. The asymmetric unit contains half a molecule of the binuclear palladium(II) complex along with two nitrates and one water molecule. The amine hydrogen atoms (of ethylenediamine) and water hydrogen atoms were located from difference Fourier maps and refined isotropically. All other hydrogen atoms were placed in geometrically idealized positions (C–H = 0.95 Å for aromatic H atoms; C–H = 0.99 Å for methylene H atoms; N-H = 0.88 Å for amide H atoms; N-H = 0.91 Å for amine H atoms) and refined isotropically.

Table S1. Summary of crystallographic data for complex **1**.

	1
Chemical Formula	C28H42N14O16 Pd2
M_r	1043.55
Temp. (K)	200(2)
Crystal system	Triclinic
Space group	*P*-1
Crystal size (mm)	0.20 x 0.15 x 0.10
a (Å)	7.7499(9)
b (Å)	10.4043(12)
c (Å)	12.9225(15)
α (°)	87.015(5)
β (°)	74.757(5)
γ (°)	75.488(5)
V (Å^3)	973.1(2)
Z D_{calc} (g cm^{-3})	1 1.781
μ(mm^{-1}) *F(000)*	8.245 528
T_{min} T_{max}	0.753 0.301
h, k, l (min,max)	(-9,9), (-11,12), (-15,15)
Reflns collected	15644
Unique reflns	3460
Observed reflns R_{int}	2854 0.0887
No. of parameters	290
GoF	1.257
$R_1[I > 2\sigma(I)]$	0.0990
$WR_2[I > 2\sigma(I)]$	0.2860
R_1_ all data	0.1082
Wr_2_ all data	0.3024
$\Delta\rho_{max}$, $\Delta\rho_{min}$ (e Å^{-3})	1.15, -2.096
CCDC No.	2168350

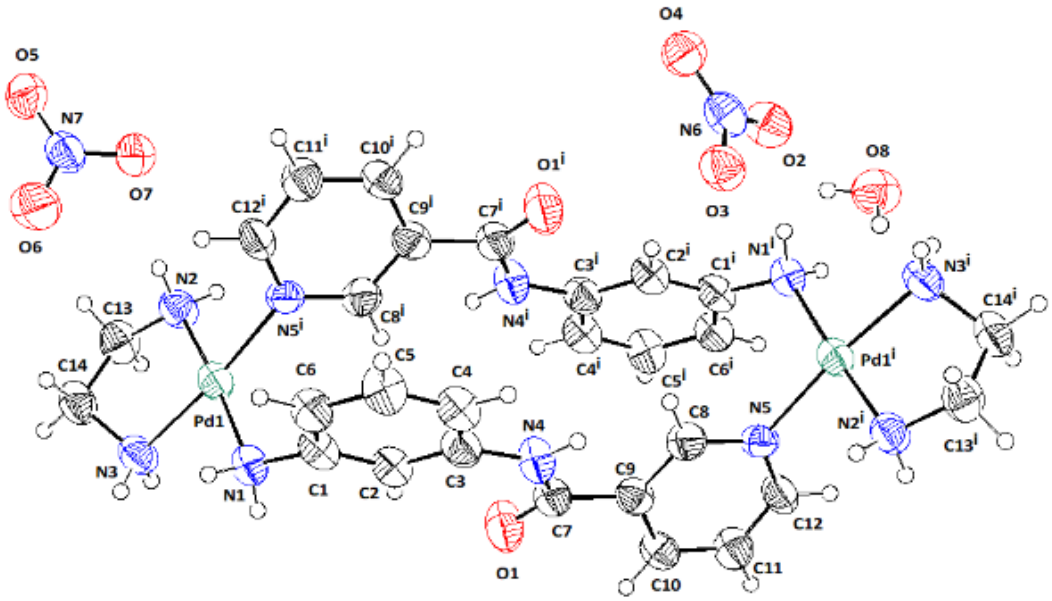

Fig. S13. ORTEP of the molecule in crystals of **1**. Thermal ellipsoids are drawn at 40% probability. Hydrogen atoms and counter anions have been omitted for clarity.

DFT Data

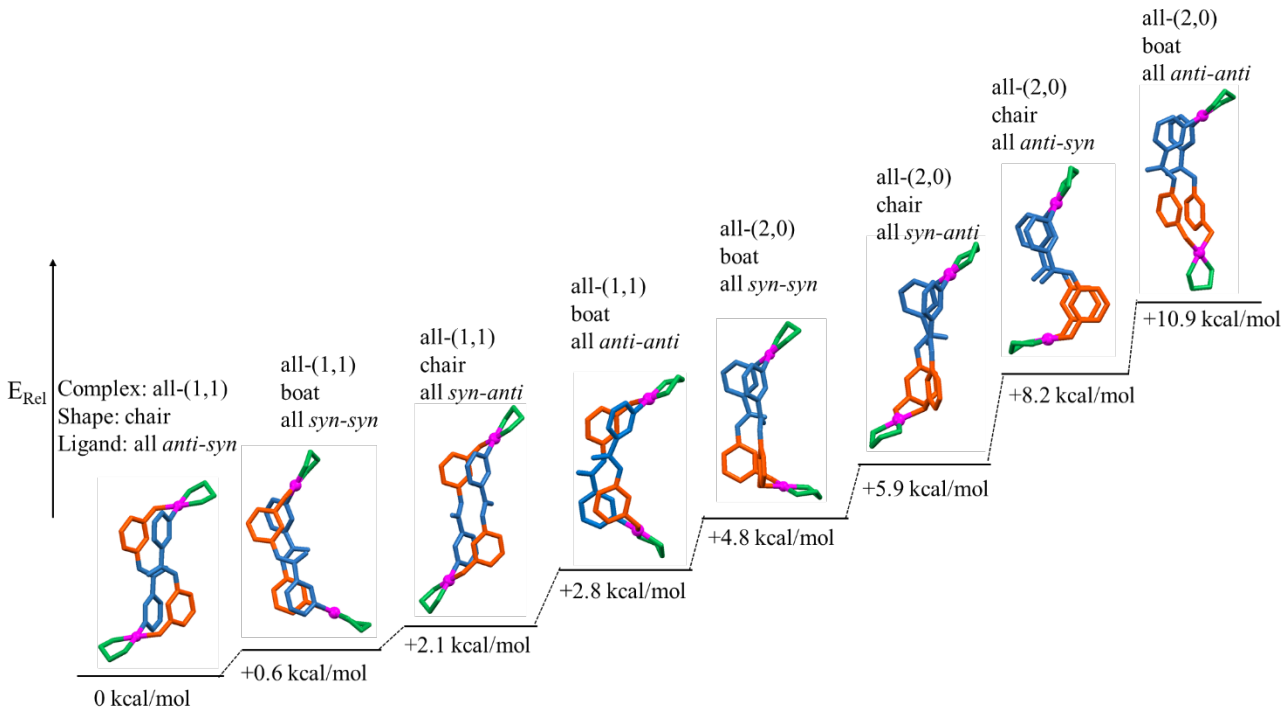

Fig. S14 Optimized geometries and relative energies of the possible isomers of $[Pd_2(en)_2(\mathbf{L}^{\mathbf{un}})_2]^{4+}$ in implicit DMSO phase.

Table S2. Energy values of the possible isomers of the complexed cation, $[Pd_2(en)_2(\mathbf{L^{un}})_2]^{4+}$ in gas phase: [B3LYP-D3/SDD,6-31G(d)].

Entry	Isomers of $[Pd_2(en)_2(\mathbf{L^{un}})_2]^{4+}$ complex in gas phase	Total Energy (in a.u.)	Total Energy (in kcal/mol)	Relative energy (in kcal/mol)
1	(1,1) Chair, *syn-anti*	-2042.698641	-1281813.023539	0
2	(1,1) boat, *syn-syn*	-2042.697461	-1281812.283077	+0.74
3	(1,1) Chair, *anti-syn*	-2042.695860	-1281811.278434	+1.74
4	(1,1) boat, *anti-anti*	-2042.669236	-1281794.571619	+18.45
5	(2,0) boat, *syn-syn*	-2042.698099	-1281812.683428	+0.34
6	(2,0) Chair, *syn-anti*	-2042.694647	-1281810.517265	+2.50
7	(2,0) Chair, *anti-syn*	-2042.671905	-1281796.246442	+16.77
8	(2,0) boat, *anti-anti*	-2042.663147	-1281790.750713	+22.27

Table S3. Energy values of the possible isomers of the complexed cation, $[Pd_2(en)_2(\mathbf{L^{un}})_2]^{4+}$ in implicit DMSO phase: [B3LYP-D3/SDD,6-31G(d)].

Entry	Isomers of $[Pd_2(en)_2(\mathbf{L^{un}})_2]^{4+}$ complex in implicit DMSO	Total Energy (in a.u.)	Total Energy (in kcal/mol)	Relative energy (in kcal/mol)
1	(1,1) Chair, *syn-anti*	-2043.391081	-1282247.536292	0
2	(1,1) boat, *syn-syn*	-2043.390149	-1282246.951453	+0.58
3	(1,1) Chair, *anti-syn*	-2043.387637	-1282245.375148	+2.16
4	(1,1) boat, *anti-anti*	-2043.386532	-1282244.68175	+2.85
5	(2,0) boat, *syn-syn*	-2043.383356	-1282242.68878	+4.8
6	(2,0) Chair, *syn-anti*	-2043.381589	-1282241.57997	+5.95
7	(2,0) Chair, *anti-syn*	-2043.378032	-1282239.347919	+8.18
8	(2,0) boat, *anti-anti*	-2043.373661	-1282236.605074	+10.93

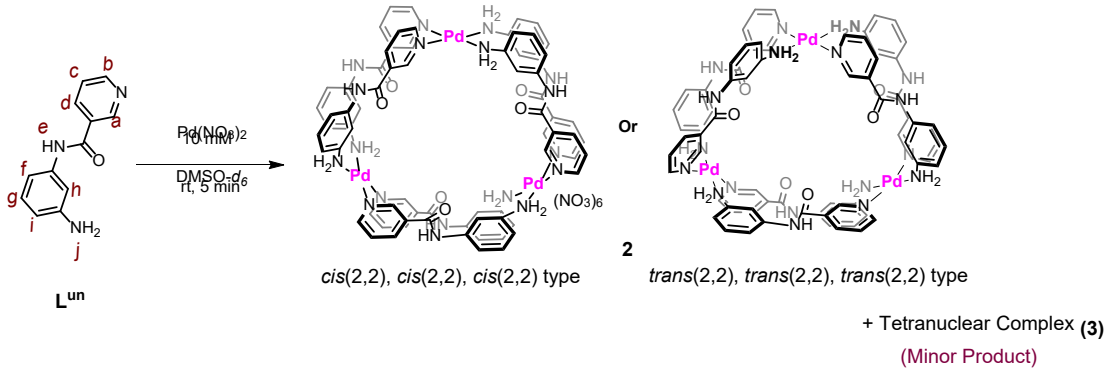

Scheme S1. Synthesis of the low symmetry trinuclear complex all-*cis*(2,2)- or all-*trans*(2,2)-$[Pd_3(\mathbf{L^{un}})_6](NO_3)_6$, **2** with minor amount of proposed low symmetry tetranuclear complex $[Pd_4(\mathbf{L^{un}})_8](NO_3)_8$, **3** (concentration: 10 Mm with respect to palladium(II)).

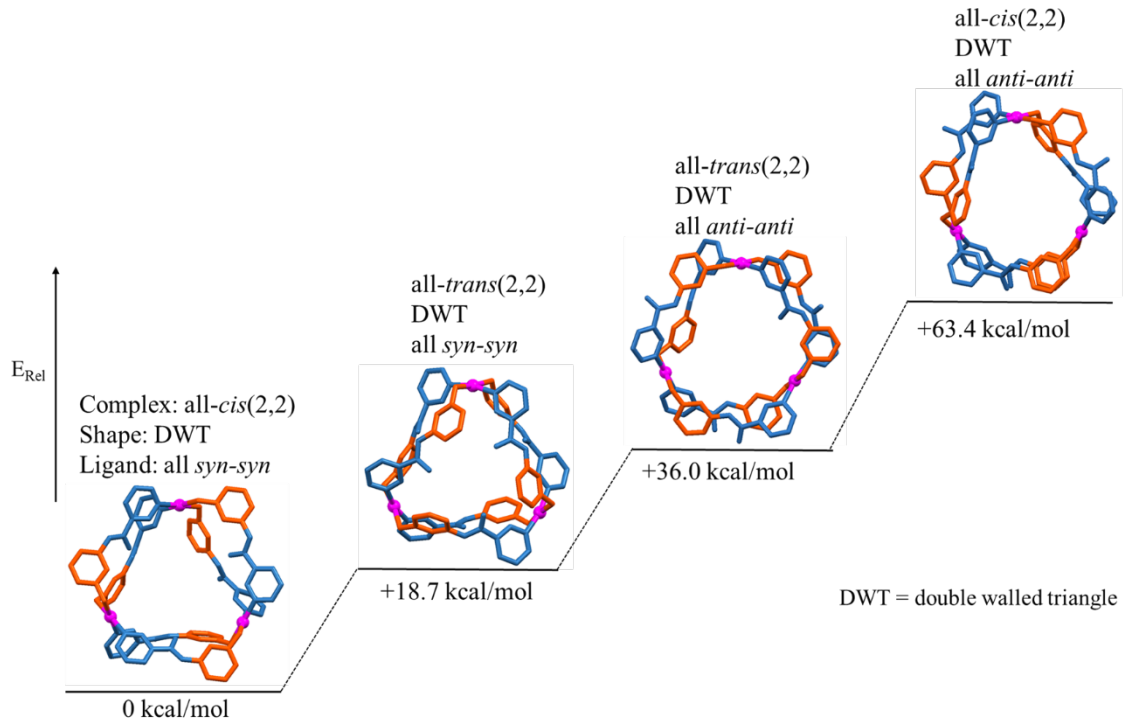

Fig. S15. Optimized geometries and relative energies of all-*cis*(2,2)-$[Pd_3(\mathbf{L^{un}})_6]^{6+}$ and all-*trans*(2,2)-$[Pd_3(\mathbf{L^{un}})_6]^{6+}$ (where ligand conformation is either all *syn-syn* or all-*anti-anti*) in gas phase.

Table S4: Energy values of the possible isomers of the complexed cation, $[Pd_3(L^{un})_6]^{6+}$: [B3LYP-D3/SDD,6-31G(d)].

Entry	**Isomers of $[Pd_3(L^{un})_6]^{4+}$ complex and condition**	**Total Energy (in a.u.)**	**Total Energy (in kcal/mol)**	**Relative energy (in kcal/mol)**
1	*cis*(2,2) Gas phase, all *syn*	-4602.501811	-2888114.107381	0
2	*trans*(2,2) Gas phase, all *syn*	-4602.471867	-2888095.317233	+18.79
3	*trans*(2,2) Gas phase, all *anti*	-4602.444439	-2888078.105899	+36.00
4	*cis*(2,2) Gas phase, all *anti*	-4602.400738	-2888050.683102	+63.42

Remarks: Conformations are assigned according to the input file. After optimisation small changes in the conformations were observed. Energy optimisation of *cis*(2,2) and *trans*(2,2) isomers of $[Pd_3(\mathbf{L^{un}})_6]^{6+}$ complex in DMSO was tried but not successful in getting the optimised structures.

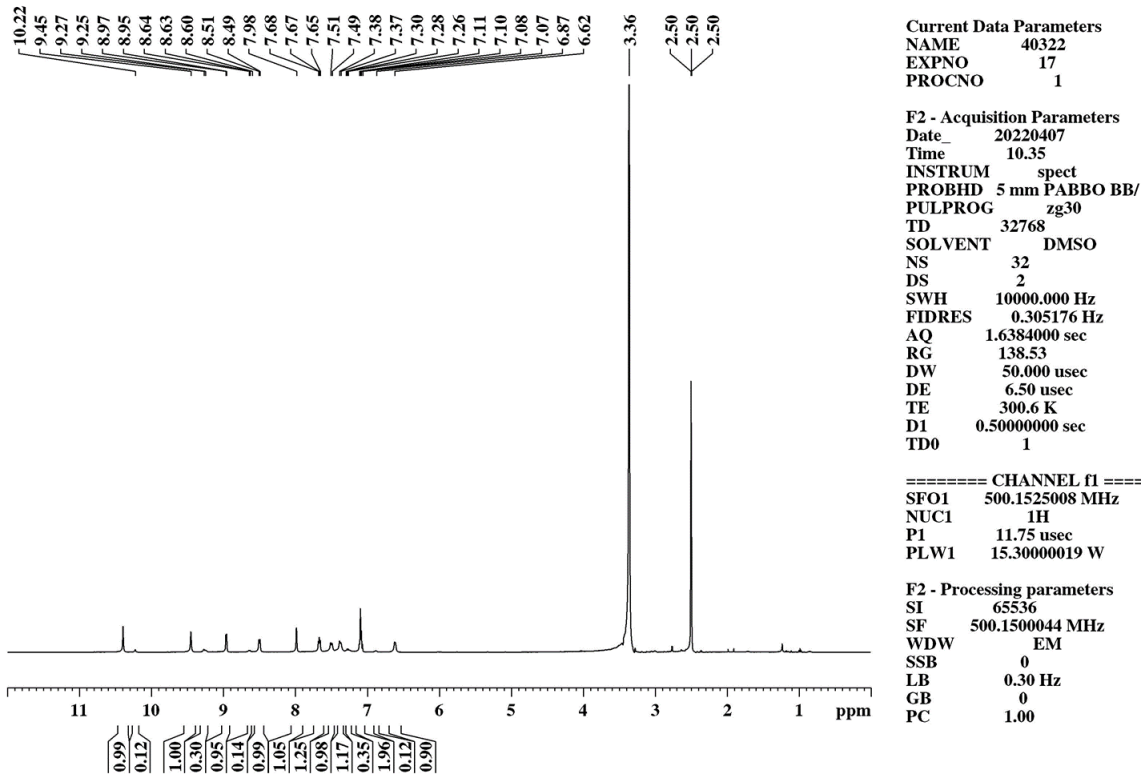

Fig. S16. 400 MHz ^{1}H NMR spectrum of complex, **2**+**3** in DMSO-d_6.

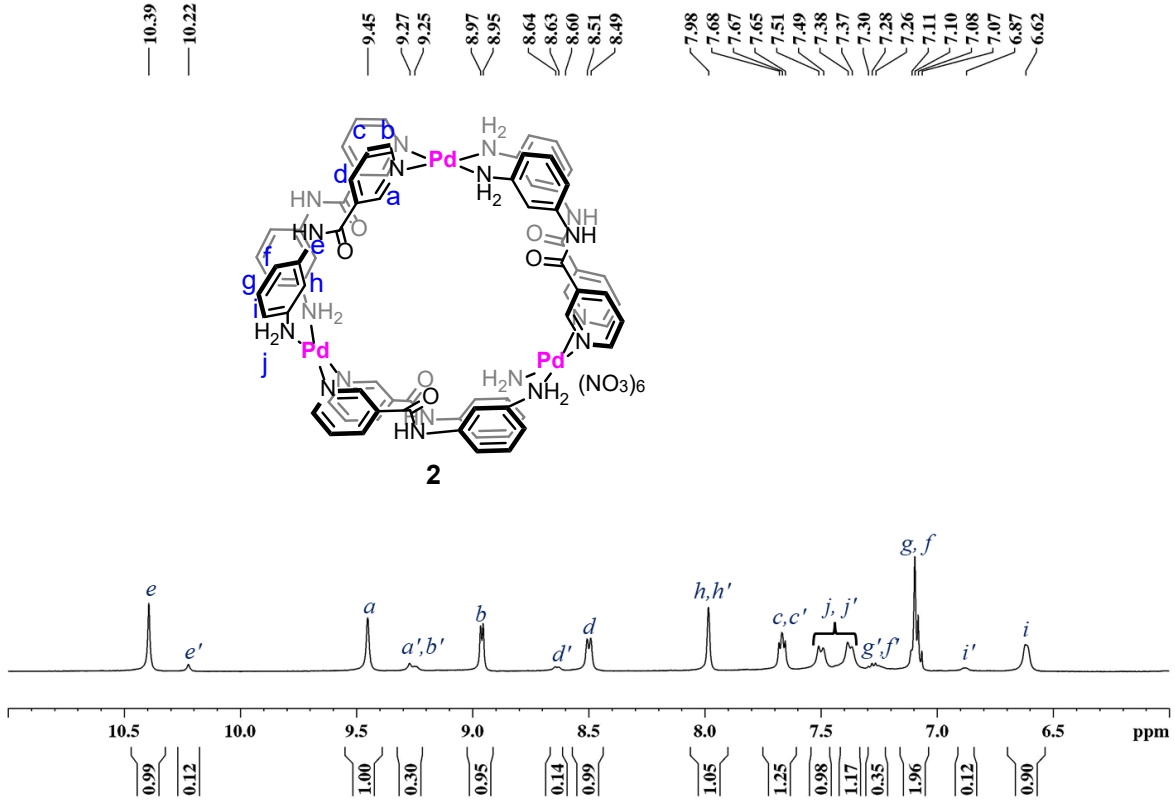

Fig. S16a. 400 MHz ^{1}H NMR expansion spectrum of complex, **2**+**3** in DMSO-d_6.

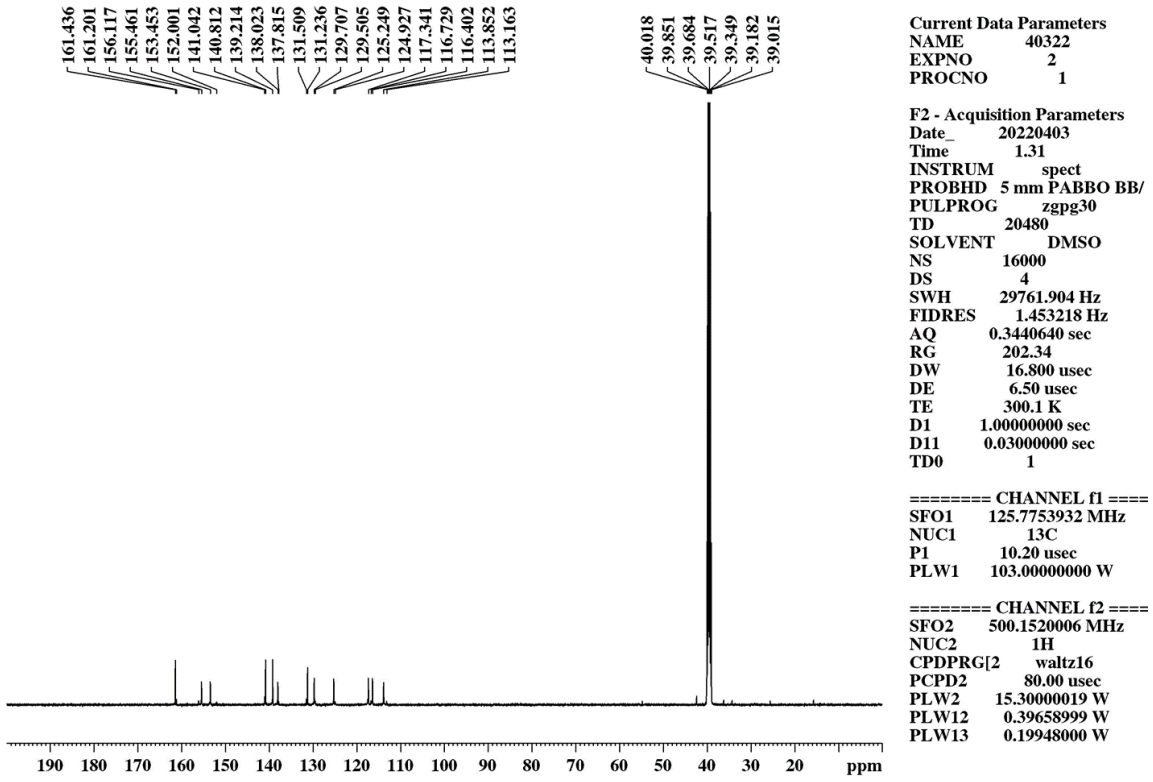

Fig. S17. 125 MHz ^{13}C NMR spectrum of complex, **2+3** in DMSO-d_6.

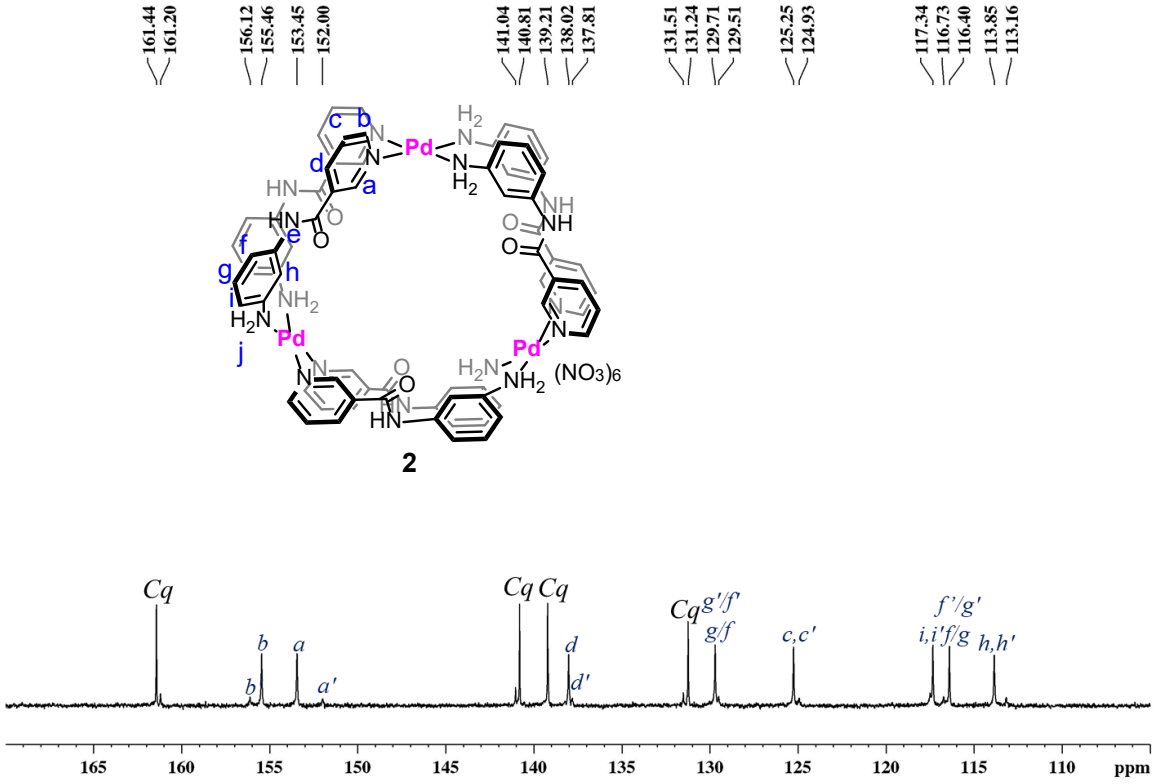

Fig. S17a. 125 MHz ^{13}C NMR expansion spectrum of complex, **2+3** in DMSO-d_6.

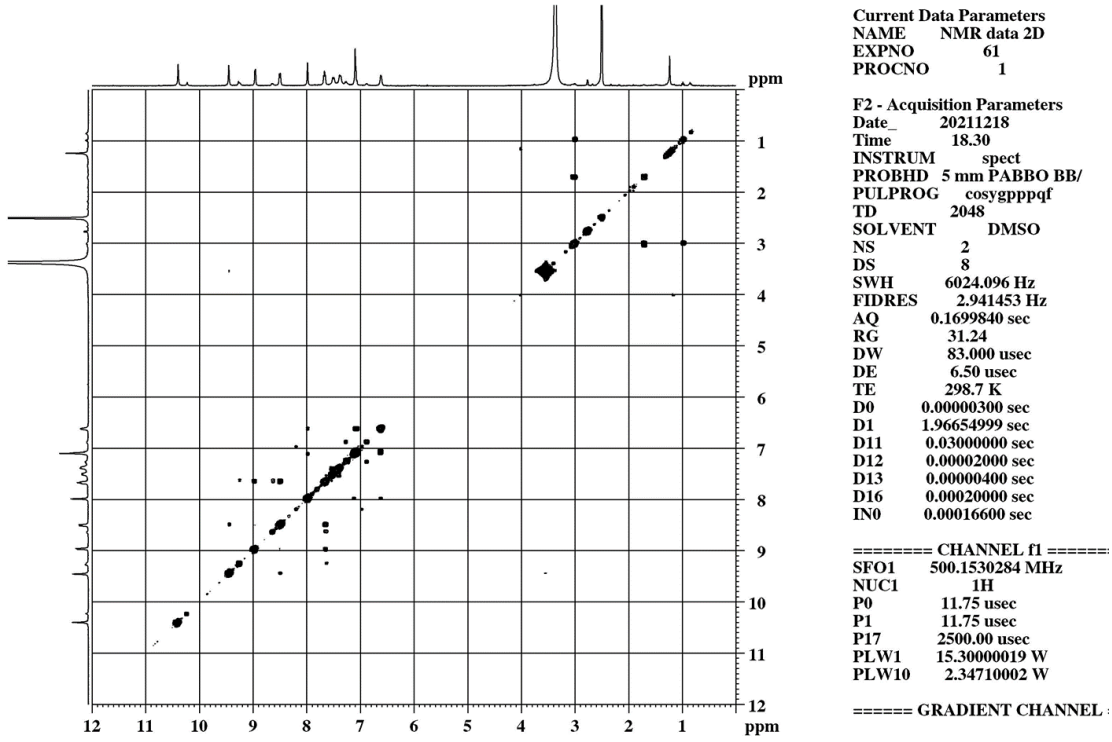

Fig. S18. 500 MHz H-H COSY spectrum of complex, **2+3** in DMSO-d_6.

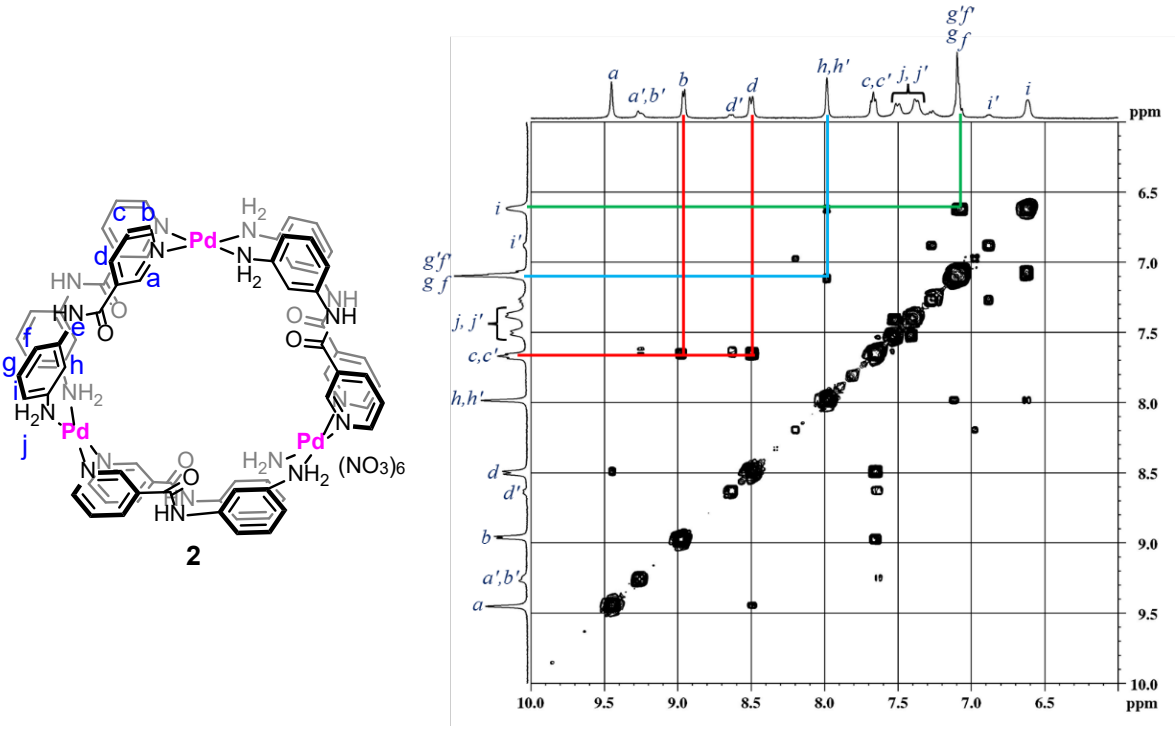

Fig. S18a. 500 MHz H-H COSY expansion spectrum of complex, **2+3** in DMSO-d_6.

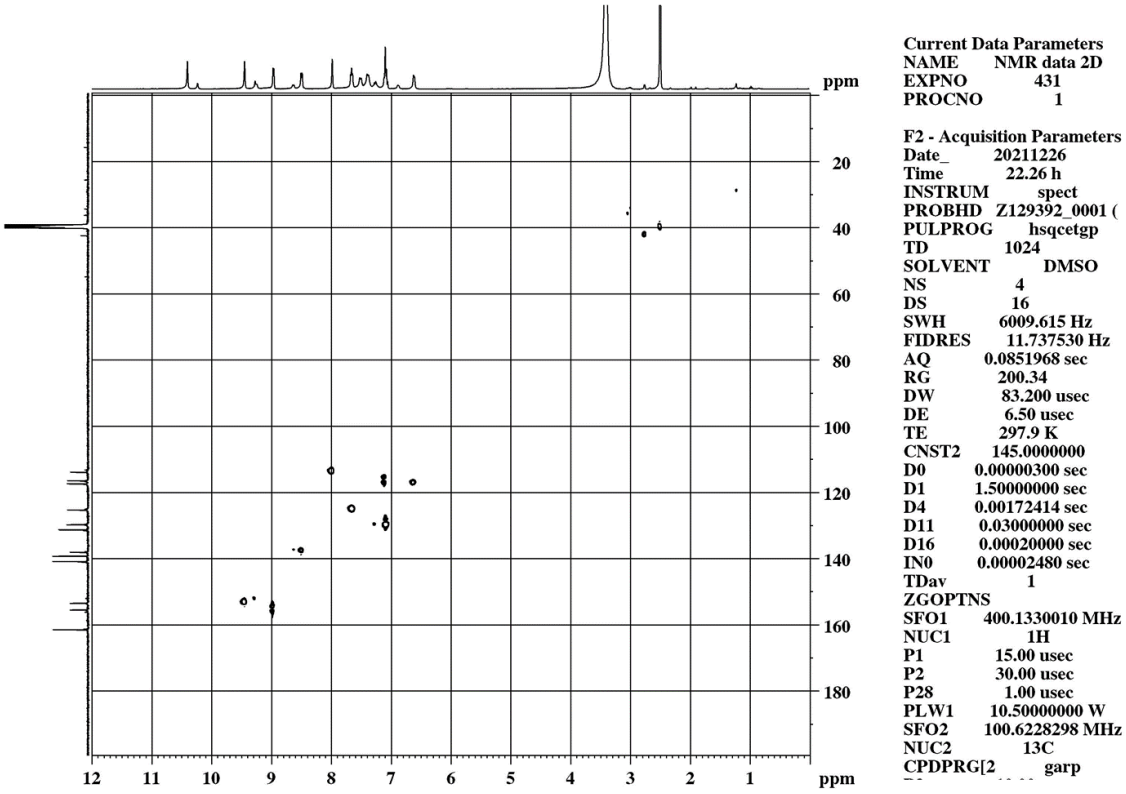

Fig. S19. 500 MHz C-H COSY spectrum of complex, **2+3** in DMSO-d_6.

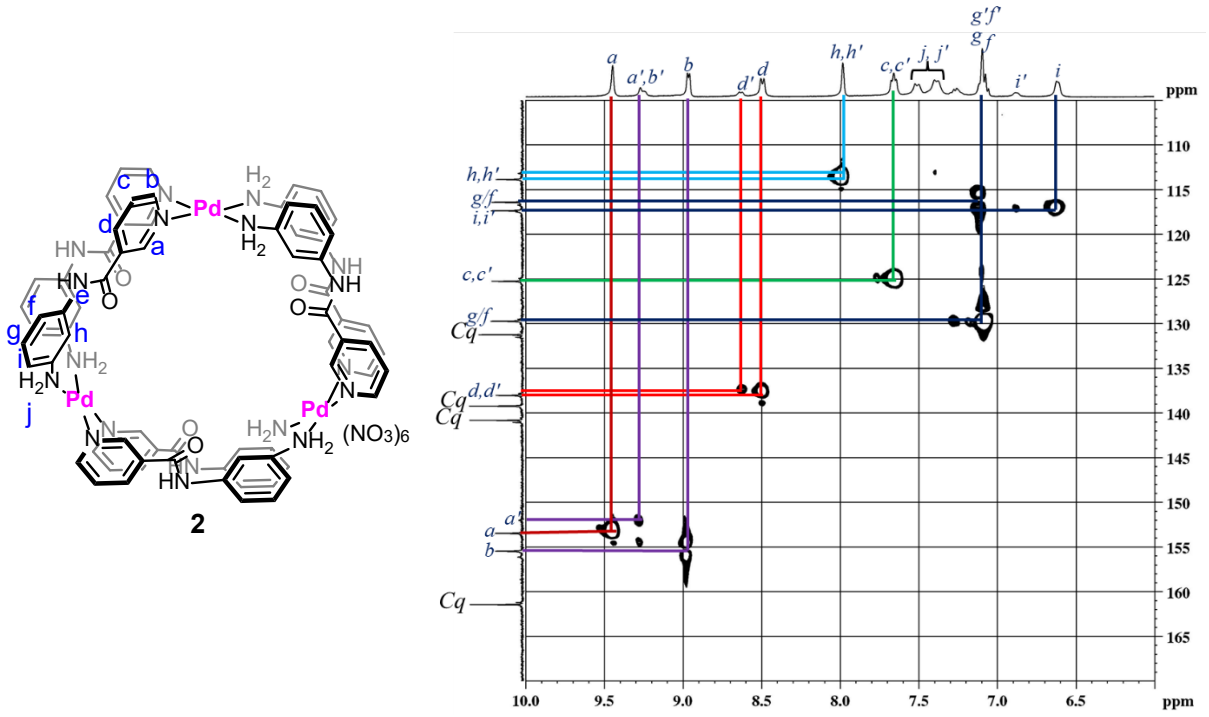

Fig. S19a. 500 MHz C-H COSY expansion spectrum of complex, **2+3** in DMSO-d_6.

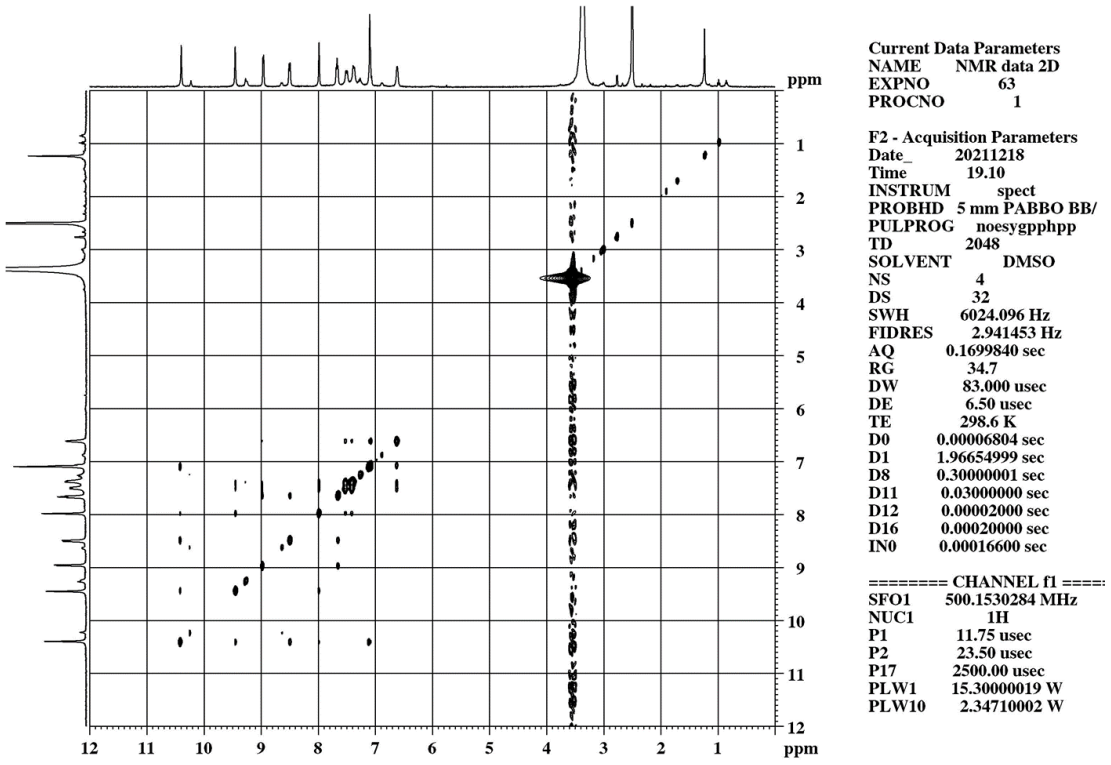

Fig. S20. 500 MHz NOESY spectrum of complex, **2**+**3** in DMSO-d_6.

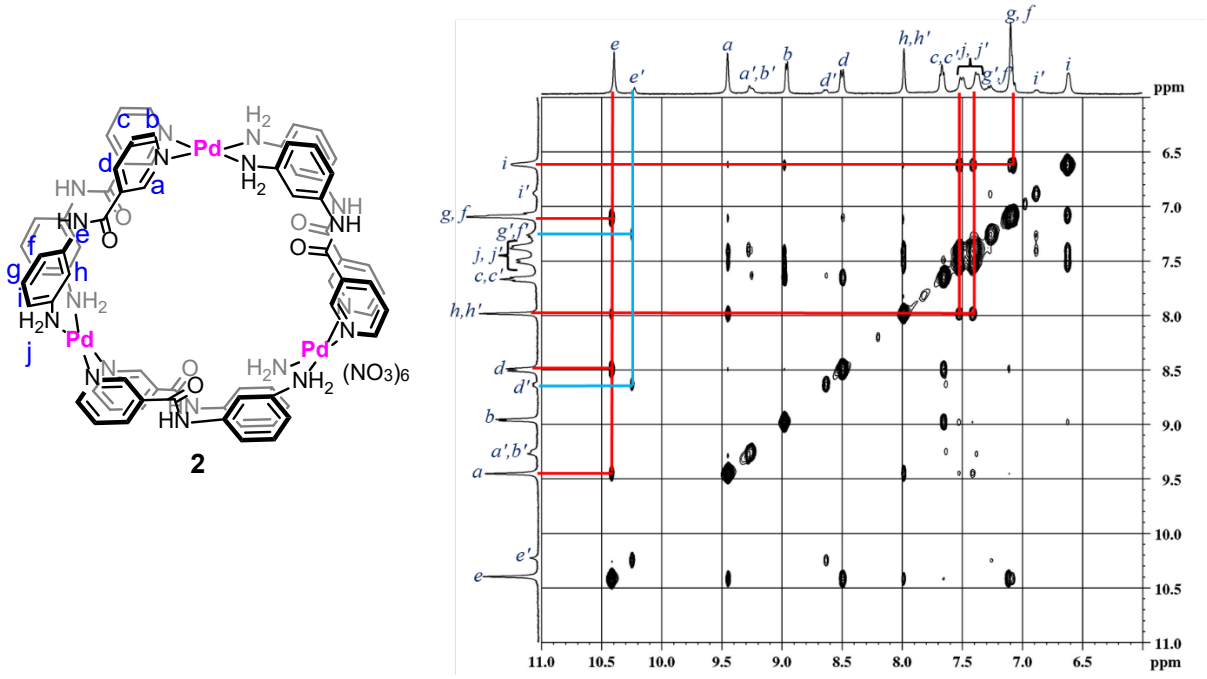

Fig. S20a. 500 MHz NOESY expansion spectrum of complex, **2**+**3** in DMSO-d_6.

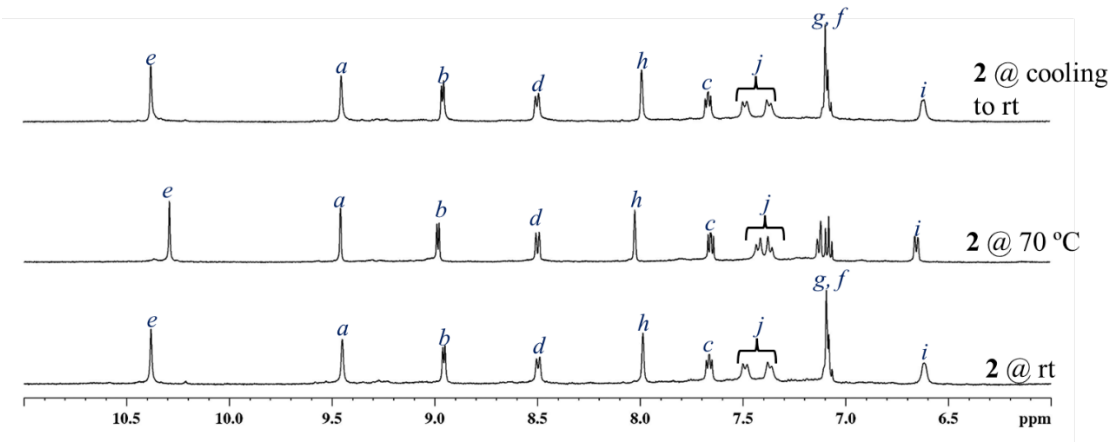

Fig. S21. Partial 400 MHz ^{1}H NMR spectra of the sample obtained from complexation of $Pd(NO_3)_2$ and ligand $\mathbf{L^{un}}$ mixed in 1:2 ratio at 2.5 mM recorded at (i) rt (ii) 70 ºC (iii) rt (reached by cooling down) in DMSO-d_6. (Concentration: 2.5 mM with respect to palladium(II)).

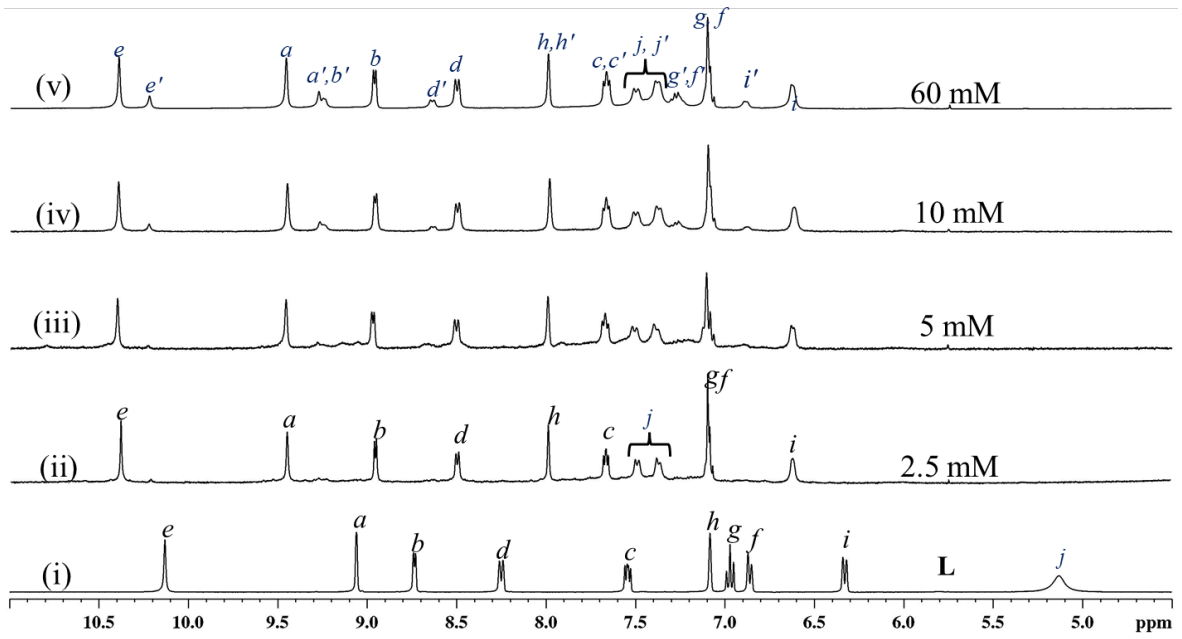

Fig. S22. Partial 400 MHz ^{1}H NMR spectra of (i) ligand, $\mathbf{L^{un}}$; (ii) to (v) sample obtained from the complexation of $Pd(NO_3)_2$ and ligand $\mathbf{L^{un}}$ mixed in 1:2 ratio at (ii) 2.5 mM; (iii) 5 mM; (iv) 10 mM; (v) 60 mM in DMSO-d_6. (Concentration: 2.5 to 60 mM range, with respect to palladium(II)).

Table S5. Approximate percentage of $\mathbf{L^{un}}$ in the complexes **2** and **3** at various concentration as calculated from integration ratio of suitable ^{1}H NMR signals.

Concentration of palladium(II)	Approximate percentage of ligand $\mathbf{L^{un}}$	
	$[Pd_3(\mathbf{L^{un}})_6](NO_3)_6$, **2**	$[Pd_4(\mathbf{L^{un}})_8](NO_3)_8$, **3**
2.5 mM	100	–
5 mM	100	Negligible
10 mM	84	16
60 mM	72	28

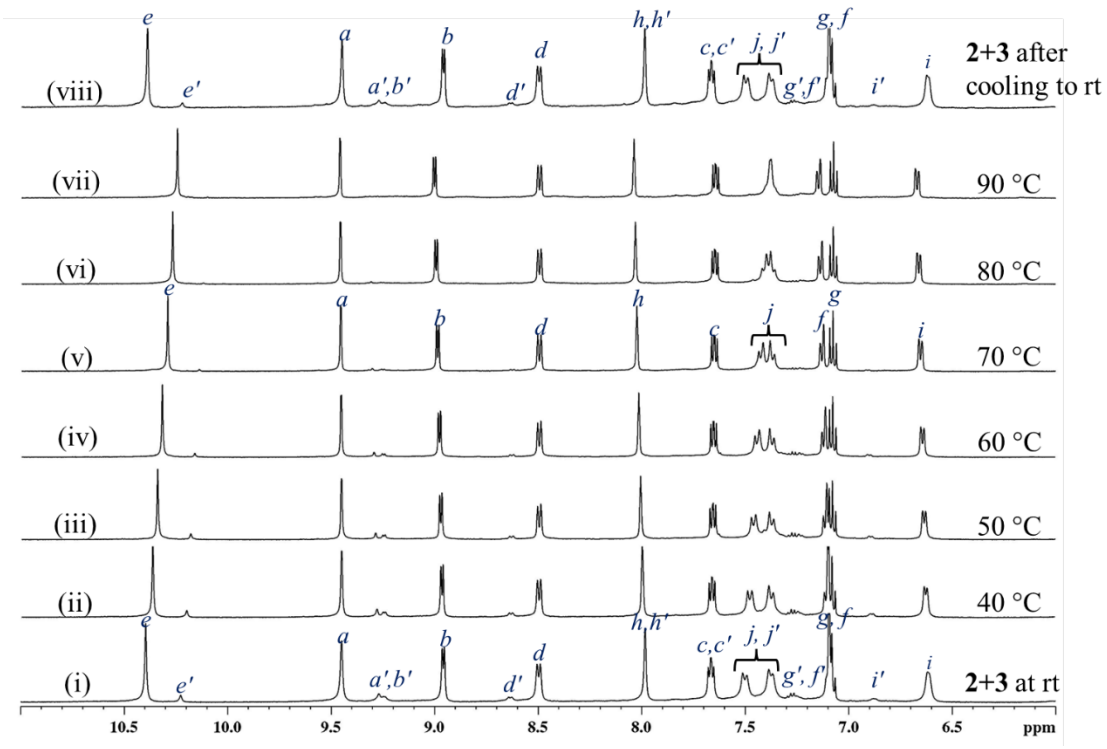

Fig. S23. Partial 500 MHz variable temperature ^{1}H NMR spectra of **2+3** recorded at (i) rt ; (ii) 40 ºC; (iii) 50 ºC; (iv) 60 ºC; (v) 70 ºC; (vi) 80 ºC; (vii) 90 ºC; and (viii) rt (reached by cooling down) in DMSO-d_6. (Concentration: 10 mM with respect to palladium(II)).

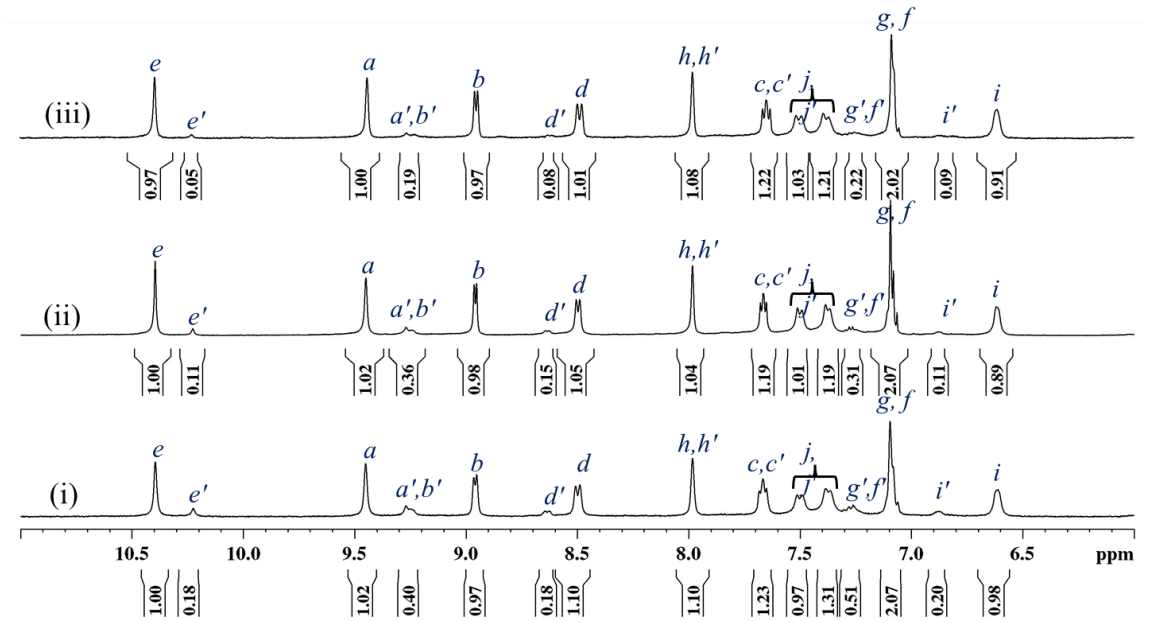

Fig. S24. Partial 400 MHz ^{1}H NMR spectra of **2+3** monitored after aging for (i) 1 d; (ii) 2 d; and (iii) 10 d in DMSO-d_6. (Concentration: 10 mM with respect to palladium(II)

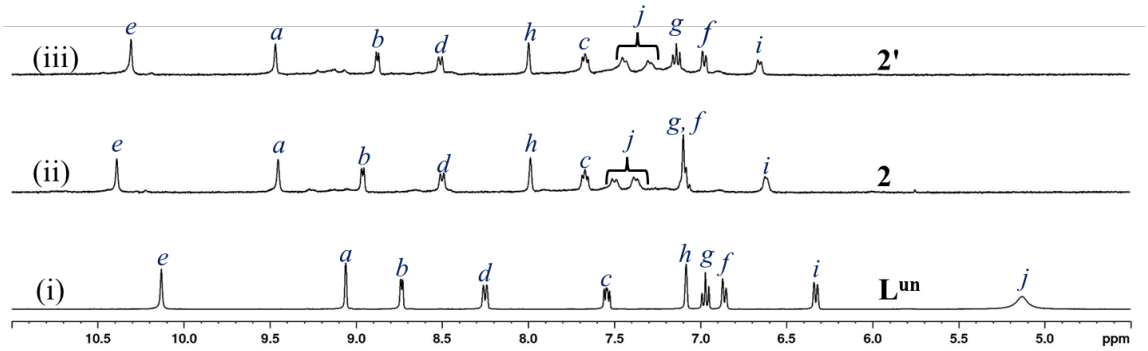

Fig. S25. Partial 400 MHz ^{1}H NMR spectra of (i) ligand $\mathbf{L^{un}}$; (ii) all-*cis*(2,2)- or all-*trans*(2,2)-$[Pd_3(\mathbf{L^{un}})_6](NO_3)_6$, **2** (iii) **all-*cis*(2,2)-** or all-*trans*(2,2)-$[Pd_3(\mathbf{L^{un}})_6](BF_4)_6$, **2'** in DMSO-$d_6$. (Concentration: 2.5 mM with respect to palladium(II))

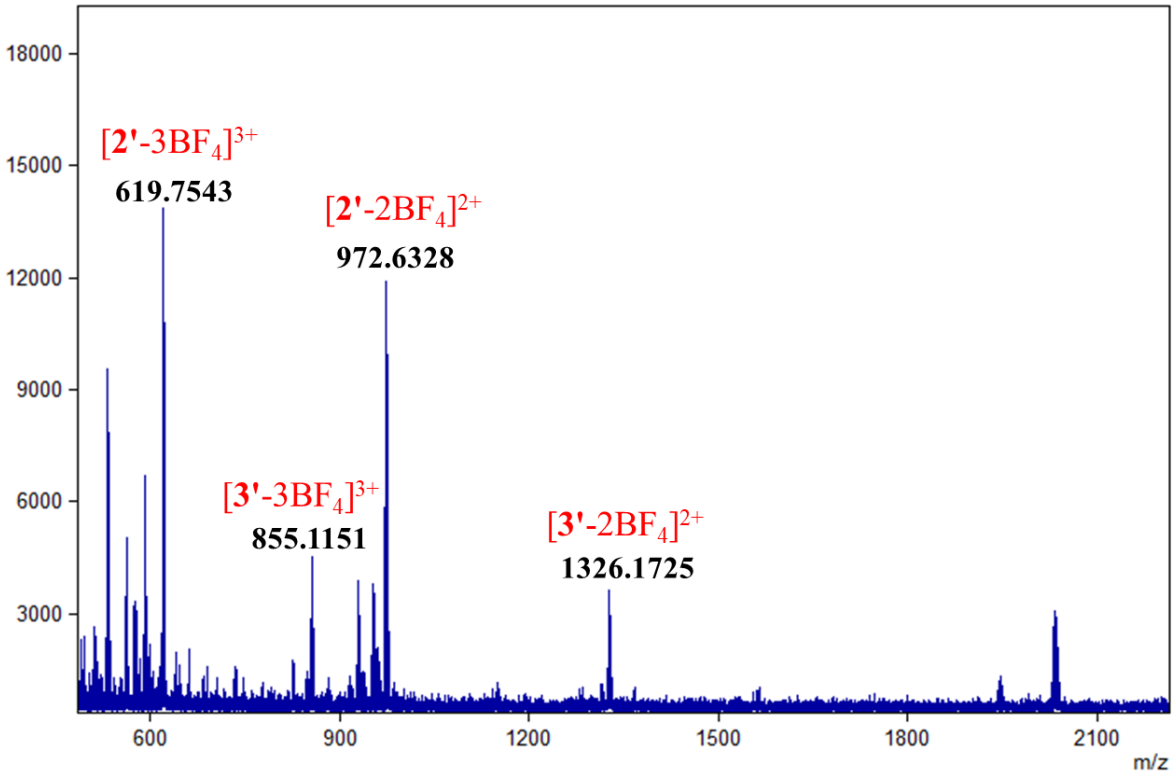

Fig. S26. ESI-MS spectrum of trinuclear complex $[Pd_3(\mathbf{L^{un}})_6](BF_4)_6$, **2'** and tetranuclear complex $[Pd_4(\mathbf{L^{un}})_8](BF_4)_8$, **3'**.

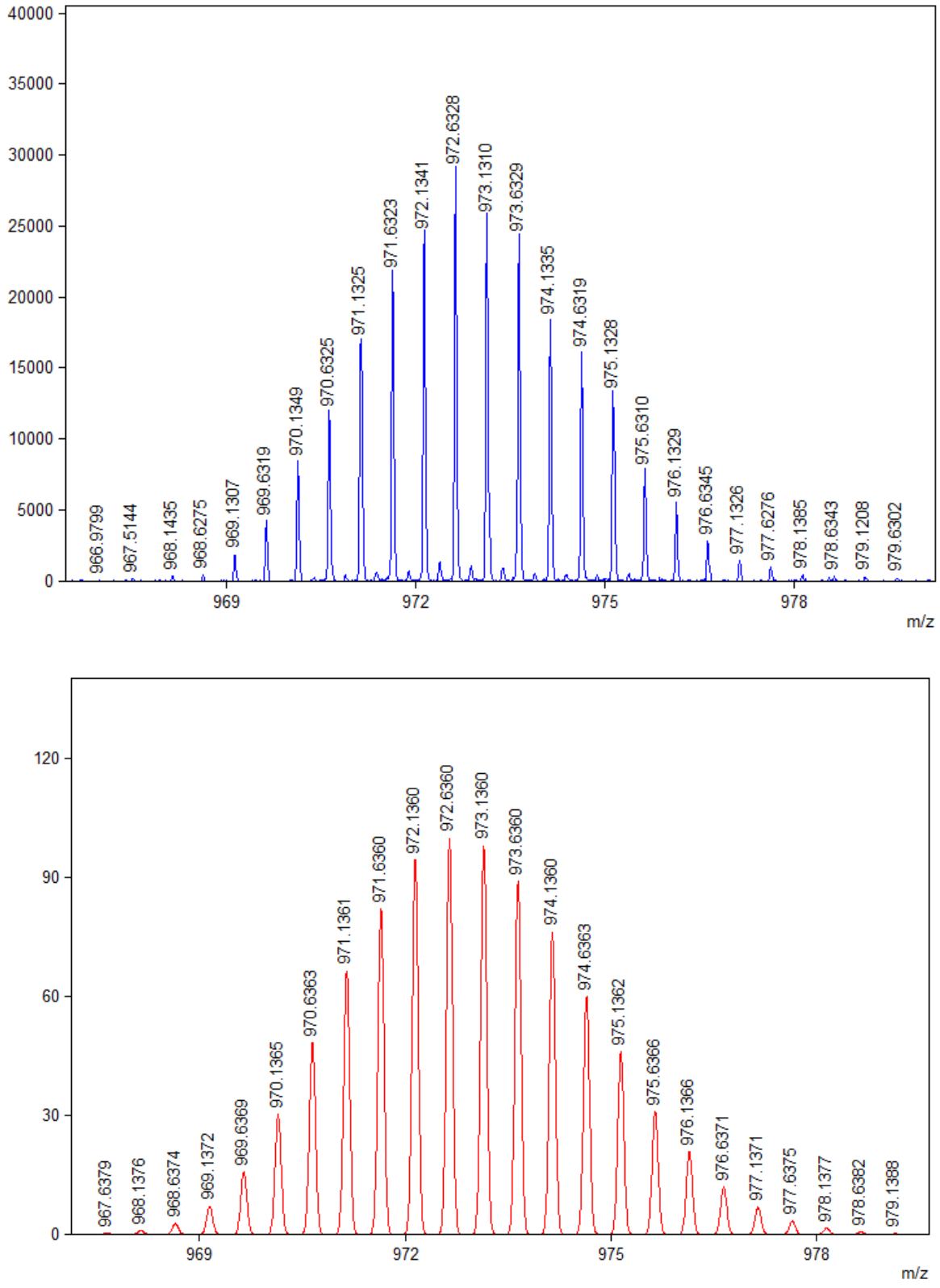

Fig. S26a. Experimental (top) and simulated (bottom) ESI-MS isotopic peak patterns corresponding to the cation [**2'**-2BF_4]$^{2+}$.

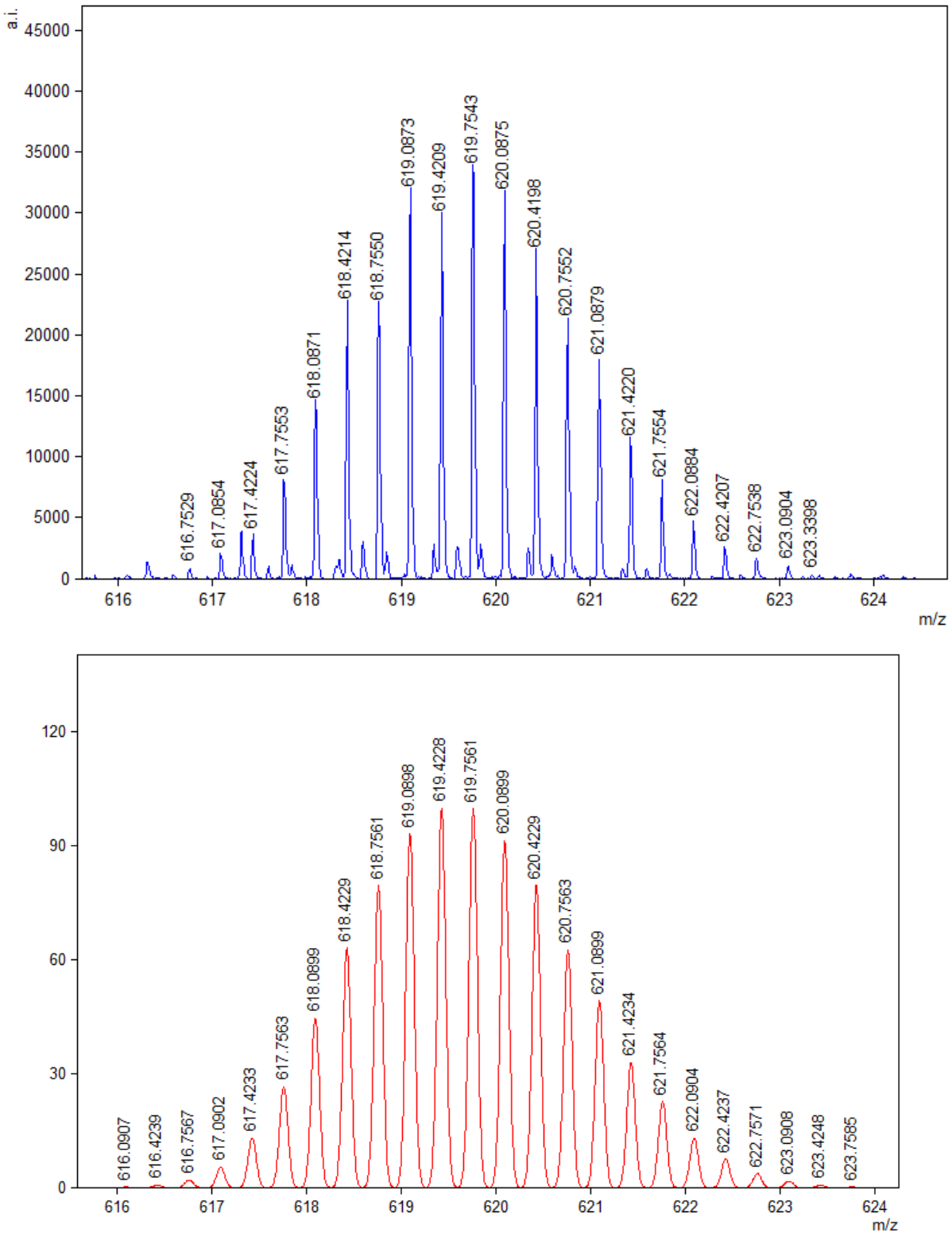

Fig. S26b. Experimental (top) and simulated (bottom) ESI-MS isotopic peak patterns corresponding to the cation [**2'**-3BF_4]$^{3+}$.

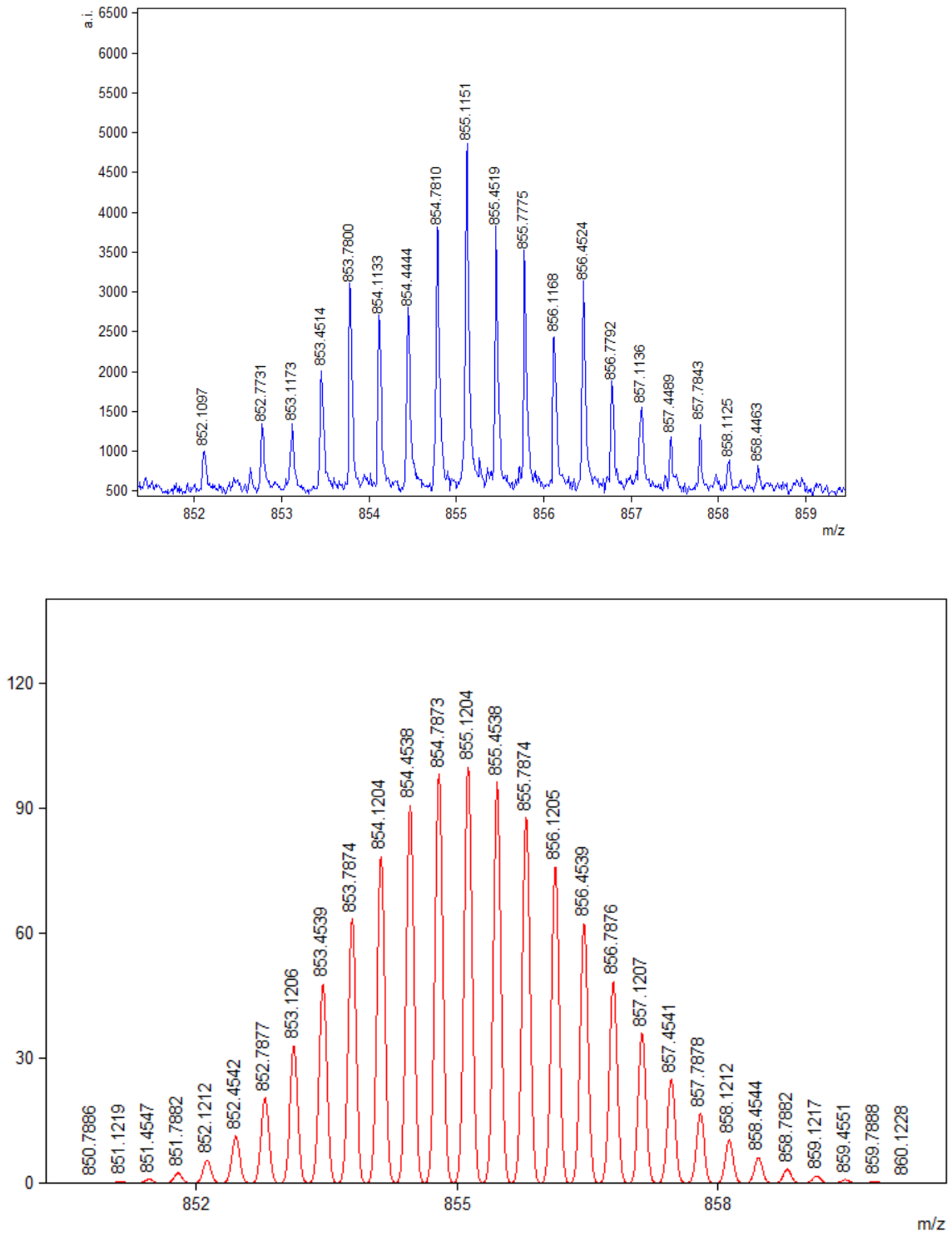

Fig. S26c. Experimental (top) and simulated (bottom) ESI-MS isotopic peak patterns corresponding to the cation [**3'**-3BF_4]$^{3+}$.

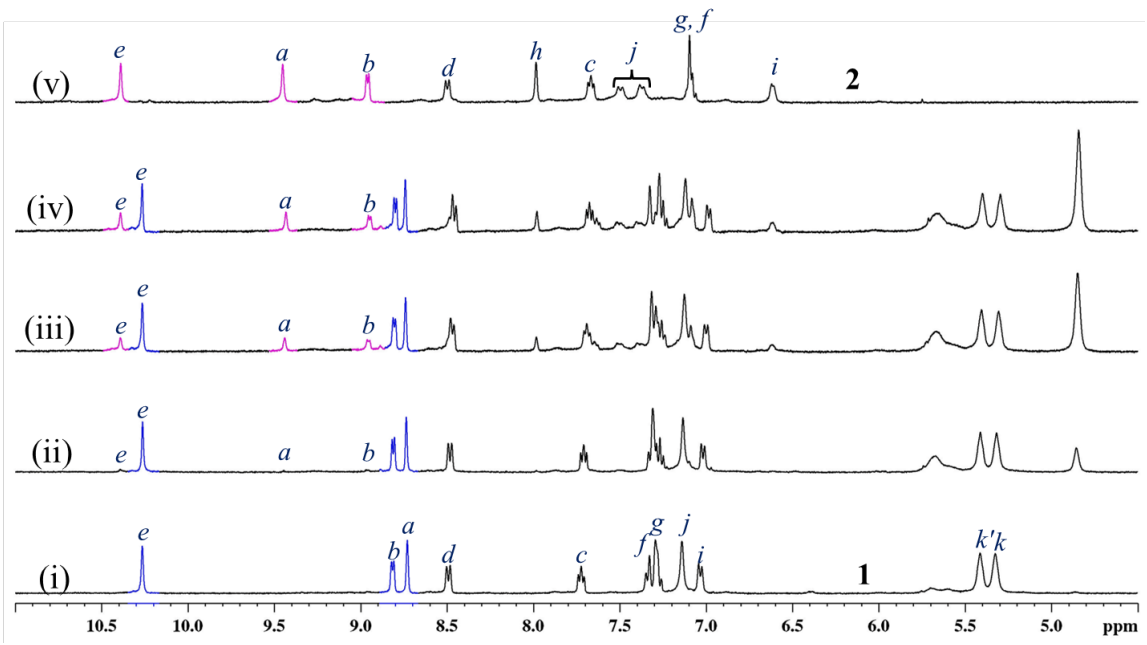

Fig. S27. Partial 400 MHz ^{1}H spectra of (i) all (1,1)-[$Pd_2(en)_2$(**L**^{un})$_2$]$(NO_3)_4$, **1**; (ii)-(iv) monitoring the formation of a mixture of all-*cis*(2,2)- or all-*trans*(2,2)-[Pd_3(**L**^{un})$_6$]$(NO_3)_6$, **2** and $Pd(en)_2(NO_3)_2$, **4** by standing a solution of **1** at ambient temperature for (ii) 3 d; (iii) 9 d; (iv) 14 d; (v) freshly prepared **2**, in DMSO-d_6. A dynamic equilibrium of **1** (65% with respect to ligand) with a mixture of **2** (35% with respect to ligand) and **4** was observed.

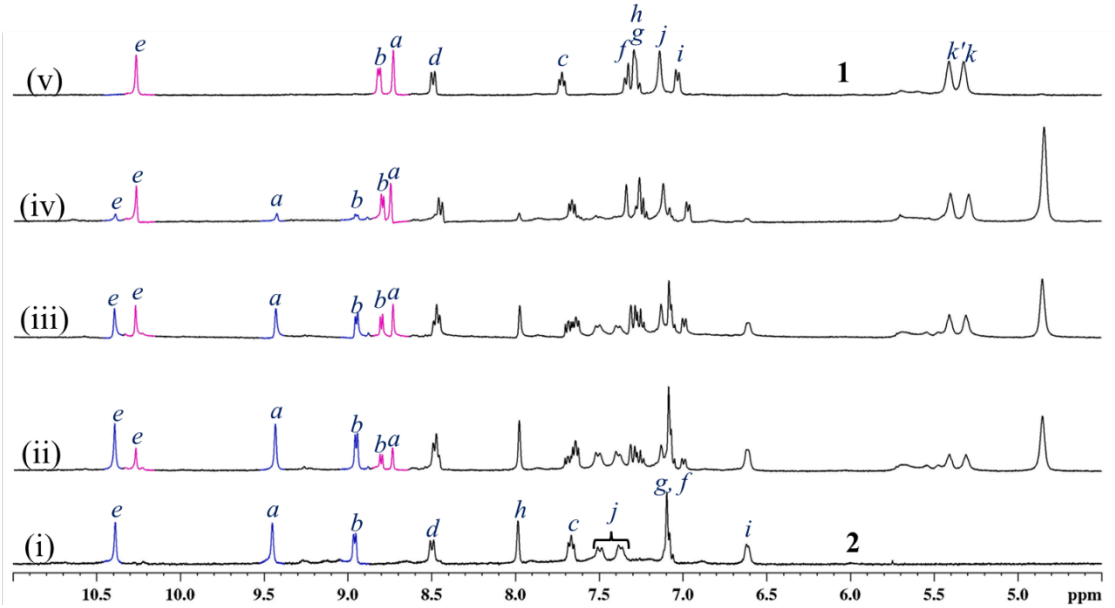

Fig. S28. Partial 400 MHz ^{1}H spectra of (i) *cis*(2,2)- or *trans*(2,2)-[Pd_3(**L**^{un})$_6$]$(NO_3)_6$, **2**; (ii)-(v) monitoring the formation of (1,1)-[$Pd_2(en)_2$(**L**^{un})$_2$]$(NO_3)_4$, **1** from a mixture of **2** and $Pd(en)_2(NO_3)_2$, **4** by standing at ambient temperature for (ii) 3 d; (iii) 6 d; (iv) 14 d; (v) freshly prepared **1**, in DMSO-d_6. A dynamic equilibrium of **1** (75% with respect to ligand) with a mixture of **2** (25% with respect to ligand) and **4** was observed.